Application of nanofiltration for acidic waters containing rare earth elements: influence of transition elements, acidity and membrane stability

J. López[a,b*], M. Reig[a,b], O. Gibert[a,b,c], E. Torres[d], C. Ayora[d], J. L, Cortina[a,b,c]

[a] *Chemical Engineering Department, UPC-BarcelonaTECH, C/ Eduard Maristany, 10-14 (Campus Diagonal-Besòs), 08930 Barcelona, Spain*

[b] *Barcelona Research Center for Multiscale Science and Engineering, C/ Eduard Maristany, 10-14 (Campus Diagonal-Besòs), 08930 Barcelona, Spain*

[c] *Water Technology Center CETaqua, Carretera d'Esplugues 75, 08940 Cornellà de Llobregat, Spain*

[d] *Institute of Environmental Assessment and Water Research (IDAEA), Consejo Superior de Investigaciones Científicas (CSIC), Jordi Girona,18, 08034, Barcelona*

[*] julio.lopez.rodriguez@upc.edu

Abstract

Acid mine drainage (AMD) is considered the main environmental problem in mining operation due to its acidity, metal content (Fe, Al, Zn, Cu) and onerous associated treatment cost. However, the presence of relatively high levels of added value elements (rare earth elements (REE)) could make its valorisation economically affordable. Membrane nanofiltration (NF) has been postulated as a potential recovery technology because it allows the recovery of a sulphuric acid rich stream and a metal rich stream in one step. In this study, the performance of a semi-aromatic polyamide NF membrane (NF270) in filtering model solutions containing common metals (Ca, Al, Zn) in sulphuric solutions (pH 1.5-3.0) was evaluated. In a second stage, the performance was assessed with the same model solutions but also containing REE. NF270 showed high rejections for metallic ions in solution, allowing acid permeation. Ion rejection data were used to determine membrane permeances to ions using the solution-diffusion model considering reactive transport. The stability of the membrane was also studied by comparing performances of a virgin membrane with an aged membrane exposed to 1 M sulphuric acid for 4 weeks. Physicochemical changes of membrane properties after ageing were also analysed by ATR-FTIR, AFM and XPS.

Keywords: NF270, sulphuric acid, rare earths, permeances, XPS, reactive transport modelling

1. Introduction

Acid Mine Drainage (AMD) is a by-product of the mining industry formed when iron sulphide minerals (e.g. pyrite (FeS_2), marcasite, (FeS_2), and pyrrhotite (FeS)) are oxidised when in contact with water and oxygen. The sulphuric acid generated has the ability to dissolve soil minerals, which leads to a high content of iron, aluminium, zinc and copper, among others, and to the presence of rare earth elements (REEs) [1]. REEs are presented in igneous and sedimentary rocks and are indispensable for the high-tech industry (e.g. power generation, X-ray imaging, fibre optics, among others) [2]. Although REEs are found in a minor proportion compared to the above-mentioned transition metals, their concentration is relatively high (two orders of magnitude higher than the one presented in natural waters) [3,4]. One of the largest sulphide ore deposits in the world is located in the Iberian Pyrite Bell (IPB), which is situated in the Southern Iberian Peninsula. More than 150 types of AMDs have been described in the Odiel and Tinto basins, which are discharged from galleries, open pits and waste dumps. It has recently been

estimated that the total discharge of AMD in the IPB watersheds is around 1 m^3/s in the dry season [5,6] with concentrations of total REEs varying from 0.3 to 11.7 mg/L with an average concentration of 1.0 mg/L [4]. Therefore, the recovery of REEs from AMD can be considered an environmentally and renewable source for their production, especially in Europe, which is lacking primary resources.

Traditional solutions to treat AMD for metal recovery are: a) neutralisation to precipitate metals as hydroxides and sulphate as gypsum [7,8]; and b) biological processing using sulphate-reducing bacteria under anaerobic conditions, leading to the precipitation of metal sulphides [9,10]. Technologies such as adsorption [11,12] and membrane-based technologies such as electro-dialysis [13,14] and nanofiltration (NF) [15-20] have been proposed as emerging solutions. NF is an attractive approach as it makes feasible acid and metal recovery in a single step taking benefit of its ability to discriminate between monovalent and multivalent ions, also allowing high acid permeation.

The application of NF membranes to treat AMD has been previously explored. Published studies reported high metal rejection rates (>85%) and high acid permeation through the membrane [15-20]. Moreover, it has been observed that higher sulphuric acid concentrations (i.e. lower pH) favour the acid passage through the membrane. This is explained by the fact that, at lower pH, a) sulphuric acid is found mainly as a monovalent ion (HSO_4^-), which has the ability to permeate more easily than the divalent ion (SO_4^{2-}), and b) functional groups of the NF membrane (e.g. carboxylic and amine groups of the piperazine) are deprotonated and, hence, single-charged anions HSO_4^- are less repelled by the membrane than double-charged anions SO_4^{2-}. However, one of the greatest concerns regarding polyamide-based membranes is the low chemical resistance of the active sites in very high acidic conditions, as described elsewhere [21–24]. Platt et al. [21] reported that the instability of membranes is a function of time exposure, temperature, type of acid and concentration. The chemical instability of NF45 and Desal DK in nitric (5% w/w) is higher than in sulphuric acid (20% w/w) after ageing for one to three months, and decreases with increasing temperature (20 to 80°C). Manis et al. [22] also reported the instability of Desal DK in 2 M sulphuric acid solutions after ageing the membrane for two months with an increase of permeate flux and a decrease of copper retention, while the MPF-34 membrane kept its properties with little variation. Navarro et al. [23] and Diallo et al. [24] aged Desal 5DL and MPF-34 membranes, respectively, in phosphoric acid and concluded that adsorbed phosphate could have an impact on selectivity by increasing polarity and modulating charge. However, ageing experiments in 2% sulphuric acid at 60°C by Tanninen et al. [25] for NF270, Desal KH and Desal-5 DK membranes showed marginal changes in pure water flux. After 3 days of immersion, Desal-5 DK exhibited a three times higher filtration flux and a decrease in copper retention, from 96 to 77%. After 7 days, all of the membranes showed more or less the same copper retention (~ 80%).

The main objective of this work was to study the performance of a piperazine-based polyamide membrane (NF270) in filtering synthetic AMD containing REEs (La, Pr, Nd, Sm, Dy and Yb) under different conditions of acidity (i.e. by varying sulphuric acid concentration), in which a pH range from 2.5 to 1.0 was studied. Experiments of membrane ageing were carried out to quantify the changes in membrane performance after being aged in 1 M sulphuric acid for 1 month. Ions rejection data were modelled with the Solution-Diffusion Model (SDM) to determine the membrane permeances to ions in solution. Equilibrium reactions at the acidity conditions of AMD (e.g. acid/base or complexing reactions) were considered. NF270 membranes were characterised by ATR-FTIR, AFM and XPS to quantify changes in membrane properties after the ageing treatment in sulphuric solutions. The novelties of this work are, on the one hand, the efforts to describe the ion transport mechanisms through the NF membrane considering ion speciation and, on the other, the effect of ageing the membrane on its performance in filtering the synthetic AMD.

2. Experimental methodology

2.1. Membranes, reagents and solutions

Experiments were carried out with samples of commercial NF270 membrane supplied by Dow Chemical. NF270 membrane is a thin film composite made up of three different layers: a piperazine semi-aromatic-based polyamide layer on the top, a polysulphone microporous support and a polyester non-woven backing layer [26,27]. Aged membranes were prepared by the immersion of NF270 sheets in a 1 M sulphuric acid solution for one month at room temperature (20°C). After this contact time membranes sheets were withdrawn from the sulphuric solution and cleaned with deionised water until the pH of the equilibrated water was close to neutrality.

Synthetic solutions were prepared by adding appropriate amounts of the metal-sulphate, nitrate, chloride and oxide salts and sulphuric acid. The following solutions and salts were used: H_2SO_4 (96 wt%, Sigma-Aldrich); $Al_2(SO4)_3 \cdot 18\ H_2O$ (55%, Panreac); $CaSO_4 \cdot 2\ H_2O$ (100%, Scharlau); $ZnSO_4 \cdot 7\ H_2O$ (100%, Panreac); $CuSO_4$ (100%, Panreac); $La_2(SO_4)_3 \cdot 9\ H_2O$ (99.9%, Alfa Aesar); $Pr(NO_3)_3 \cdot 6\ H_2O$ (100% Fluka AG); $NdCl_3 \cdot 6\ H_2O$ (100%, Fluka AG); $SmCl_3$ (100%, Fluka AG); Dy_2O_3 (99.9%, Fluka AG) and Yb_2O_3(99.9% Fluka AG).

2.2. Membrane cross-flow experimental set-up

The experimental set-up has been previously described in [28]. Experiments were carried out with NF270 membrane (0.014 m^2), which was placed in a test cell (GE SEPA^{TM} CF II) with a spacer-filled feed channel, and with the possibility to vary the cross-flow velocity (cfv) and trans-membrane pressure (TMP). The solution was kept at a constant temperature (25 ± 2°C) in a thermostated 30 L tank and it was pumped into the cross-flow cell with a high pressure diaphragm pump (Hydra-Cell, USA) at prefixed required flow rates and pressures. A manometer was located at the entrance of the test cell. Both outputs of the cell (retentate and permeate) were recycled back to the tank to keep a constant concentration in the feed solution. The system was provided with a needle and a by-pass valve to vary the cfv, which was fixed, and the TMP. The first was located at the retentate stream, just at the exit from the test cell. The concentrate passed through a manometer and a flow meter. Just before the discharge of the retentate to the tank, a pre-filter cartridge (100 µm, polypropylene) was placed to avoid erosion products reaching the pump and to eliminate microorganisms. Permeate samples were collected by a three-way valve. Pipes were made of stainless steel.

Membranes were placed in Milli-Q water overnight to remove conservation products. The membrane was compacted at 22 bar and cfv of 1 m/s with deionised water and with the working solution for 2 h and 1.5 h, respectively. Experiments were carried out at a pre-fixed cfv (0.7 m/s) and TMP was varied. Conductivity was measured on-line in the permeate stream and samples were taken when conductivity was stable. Once the experiment was finished, the membrane was cleaned with deionised water at 10 bar for 30 min and at 20 bar for 1.5 h.

Permeate samples were analysed with a conductivity-meter and a pH-meter. A data acquisition system was programmed in LABVIEW® version 8.6 (Laboratory Virtual Instrumentation Engineering Workbench), which collected data from the flow-meter and the pressure-meter.

2.3. Experimental design for membrane performance in sulphuric solutions

Experiments were performed over a range of pH (1.0 - 2.5) in order to reproduce different acidities typical of AMD. In the first group of experiments (1 to 4 in Table 1), a virgin sample of NF270 was used and the model solutions included four main components: a strong acid (sulphuric acid), a trivalent transition metal ion (Al), a divalent transition metal ion (Zn) and a rare alkaline metal ion (Ca). By increasing the sulphuric acid concentration, pH was varied from 2.5 to 1.0.

Synthetic solutions simulating the supernatant of a pre-treated AMD from La Poderosa Mine at the Iberian Belt (Huelva SW Spain) after being treated by limestone to remove Fe(III) were filtered (experiments 4 and 5). Pre-treatment excluded the removal of Al at pH higher than 4, because REEs are entirely precipitated with the Al-solid basaluminite ($Al_4SO_4(OH)_{10}{\cdot}5H_2O$). The whole pre-treatment process is described in detail by Ayora et al. [4]. Typically, the concentrations of REE in AMD range from 0.2 up to 5 mg/L, which are around one to two orders of magnitude lower than the main transition metal ions (20 mg/L Zn to 580 mg/L Al). REEs (La, Pr, Nd, Sm, Dy and Yb) were added to the solution, which was then filtered using a virgin and an aged membrane in 1 M sulphuric acid solution for one month.

Table 1. Experimental details on the NF270 assays with virgin and aged membranes

Experiment	**1**	**2**	**3**	**4**	**5**
$pH_{initial}$	2.5	1.9	1.5	1.0	1.0
Membrane	Virgin	Virgin	Virgin	Virgin	Aged
$H_2SO_{4\ inl}$ (mM)	18.4	25.1	39.4	84	84
IS (ionic strength, mM)	52	66	96	169	169
$[Al]_{TOT}$ (mM)	12.4	12.7	12.6	20.7	20.7
$[SO_4^{2-}]_{TOT}$ (mM)	26.7	33.5	47.9	97.8	97.8
$[Zn]_{TOT}$ (mM)	0.65	0.65	0.65	0.71	0.71
$[Ca]_{TOT}$ (mM)	6.0	6.0	6.7	0.59	0.59
$[Cu]_{TOT}$ (mM)				0.6	0.6
$[La]_{TOT}$ (mM)				0.068	0.068
$[Pr]_{TOT}$ (mM)				0.072	0.072
$[Nd]_{TOT}$ (mM)				0.064	0.064
$[Sm]_{TOT}$ (mM)				0.045	0.045
$[Dy]_{TOT}$ (mM)				0.063	0.063
$[Yb]_{TOT}$ (mM)				0.043	0.043

2.4. Membrane characterisation methodologies

The NF270 membrane functional groups were characterised by ATR-FTIR spectroscopy (JASCO FT/IR-4100) with sixty-four scanning times, providing a resolution of 4 cm^{-1}. The elementary composition of membrane active layer was analysed by an X-ray photo electron spectroscopy (XPS, SPECS system) using an Al anode XR50 source operating at 150 W and a Phoibos MCD-9 detector at vacuum lower than 10^{-8} mbar. The area of analysis was 0.8 mm^2 and accuracy of binding energies was 0.1 eV. Membrane samples were completely dried under vacuum at 40°C for 4 h before XPS and ATR-FTIR characterization.

Static contact angles were measured by a contact angle goniometer (OCA15EC, Dataphysics, Germany) equipped with a video camera. Water droplet morphologies and contact angles were analysed by the SCA 202 software (Dataphysics). At least five water contact angles at different locations on one membrane surface were averaged to obtain a reliable value. Streaming potential measurements were performed by Anton Paar GmbH (Graz, Austria) with the SurPASS Adjustable Gap Cell in presence of a 1 mM solution of KCl as background electrolyte at pH values from 2.5 to 5, which was adjusted with 0.1 M HCl or 0.1 M NaOH solutions. For each measurement, a pair of membrane pieces (cross section of 20 × 10 mm^2) was used. The membrane zeta potential was calculated by the Helmholtz– Smoluchowski equation [29].

Surface roughness analysis was performed by atomic force microscopy (AFM, Multimode Veeco V) using contact mode in air. The scanning area was 1x1 µm. The membrane samples were completely dried under vacuum at 40°C for 24h before the SEM and AFM measurements. Nanoscope software was used to collect and analyse the images.

Aqueous Solutions Chemical Analyses

The pH and electrical conductivity were measured in situ. Filtered samples (0.1 µm nylon) were acidified with HNO_3 and diluted appropriately for the analysis of major (Al, Ca, Zn, Cu, S) and REEs by inductively coupled plasma atomic emission spectroscopy (ICP-AES, Perkin-Elmer® Optima 3200 RL) and inductively coupled plasma mass spectroscopy (ICP-MS, Perkin-Elmer® SciexElan 6000), respectively.

3. Ion-transport modelling through NF membranes from sulphuric acid solutions

Modelling of ion rejection was carried out using the Solution-Diffusion Model (SDM) [30–33]. Ion flux was described according to Niewersch et al. [34,35] assuming that there is no coupling between solute and solvent flow inside the membrane and then the reflection coefficient is assumed to be equal to one. Recent studies have shown that in RO and NF membranes, the convective coupling of solvent flux and ions in the membrane phase is very weak [36–38]. Ion flux is described according to the following equation (Eq. 1):

$$j_i = -P_i \cdot \left(\frac{dc_i}{dx} + c_i \cdot \frac{d(\ln \gamma_i)}{dx} + z_i \cdot c_i \cdot \frac{d\varphi}{dx}\right) \text{(Eq. 1)}$$

Where j_i is the flux of component i through the membrane, x is the dimensionless position in the membrane, P_i is the membrane permeance to ion i, c_i is the concentration of component i, γ_i is the activity coefficient of component i, z_i is the valence charge of component i and φ is the dimensionless virtual electrostatic potential in the membrane. The activity coefficient was calculated by using the Davies Equation (Eq.2):

$$\log \gamma_i = -a^* \cdot z_i^2 \cdot \left(\frac{\sqrt{IS}}{1+\sqrt{IS}} - 0{,}3 \cdot IS\right) \text{(Eq.2)}$$

The approach uses “virtual concentrations”, which are defined as those which are in thermodynamic equilibrium with an infinitely small fluid volume inside the membrane [32,35]. Membrane permeance to ion is a function of thermodynamic diffusion coefficient inside the membrane, partitioning at the surface membrane-solution and membrane properties [34,35]. Due to the dependence of the diffusion coefficient on concentration, membrane permeance to ions will also depend on it. Nevertheless, membrane permeances across the membrane, as a preliminary hypothesis, are assumed to be constant. By simplicity, concentration polarisation was not taken into account.

Due to the existence of chemical reactions between the different species in solution, mass transport equations are referred to the total concentration of the component in solution. These equations will include all of the species of a given component which are present in the solution. The species are also subjected to the electro-neutrality condition (Eq.3):

$$\sum_{i=1}^{n}(z_i \cdot c_i) = 0 \text{ (Eq.3)}$$

From the measured total ion concentrations and equilibrium constants, the concentration of each species was determined. Mass balance equations were solved using Matlab®, in which the membrane permeances to ions were varied by minimising the error between the total rejection of one component obtained experimentally and the one obtained from the model. Total component or individual ion rejection (R) is defined according to (Eq.4):

$$R = 1 - \frac{C_p}{C_f} \text{ (Eq.4)}$$

Where C_p and C_f represent the total concentration regardless of its speciation or the individual concentration of one specie in the feed and permeate streams, respectively.

Mass balance equations were written for each element in solution: H, S, Al, and so on. In Annex I, chemical speciation of the filtered solutions is presented (diagrams were built with the Hydra/Medusa Code [39]). The main equilibrium constants of the metal-sulphate complexes from the Hydra data base [39] are summarised in Table 2.

Table 2. Chemical equilibrium constants for the species in the solution (Hydra database) [39]

Chemical reaction	$\mathrm{pK} = -\log \mathrm{K_{T,I}}$	Chemical reaction	$\mathrm{pK} = -\log \mathrm{K_{T,I}}$
$H^+ + SO_4^{2-} \leftrightarrow HSO_4^-$	1.98	$Pr^{3+} + SO_4^{2-} \leftrightarrow PrSO_4^+$	3.62
$Al^{3+} + SO_4^{2-} \leftrightarrow AlSO_4^+$	3.50	$Pr^{3+} + 2\,SO_4^{2-} \leftrightarrow Pr(SO_4)_2^-$	4.90
$Al^{3+} + 2\,SO_4^{2-} \leftrightarrow Al(SO_4)_2^-$	5.00	$Nd^{3+} + SO_4^{2-} \leftrightarrow NdSO_4^+$	3.64
$Ca^{2+} + SO_4^{2\pm} \leftrightarrow CaSO_4$	2.30	$Nd^{3+} + 2\,SO_4^{2-} \leftrightarrow Nd(SO_4)_2^-$	5.10
$Ca^{2+} + H^+ + SO_4^{2-} \leftrightarrow CaHSO_4^+$	3.07	$Sm^{3+} + SO_4^{2-} \leftrightarrow SmSO_4^+$	3.65
$Cu^{2+} + SO_4^{2-} \leftrightarrow CuSO_4$	2.31	$Sm^{3+} + 2\,SO_4^{2-} \leftrightarrow Sm(SO_4)_2^-$	5.20
$Zn^{2+} + SO_4^{2-} \leftrightarrow ZnSO_4$	2.37	$Dy^{3+} + SO_4^{2-} \leftrightarrow DySO_4^+$	3.61
$Zn^{2+} + 2\,SO_4^{2-} \leftrightarrow Zn(SO_4)_2^{2-}$	3.28	$Dy^{3+} + 2\,SO_4^{2-} \leftrightarrow Dy(SO_4)_2^-$	5.10
$La^{3+} + SO_4^{2-} \leftrightarrow LaSO_4^+$	3.62	$Yb^{3+} + SO_4^{2-} \leftrightarrow YbSO_4^+$	3.59
$La^{3+} + 2\,SO_4^{2-} \leftrightarrow La(SO_4)_2^-$	5.10	$Yb^{3+} + 2\,SO_4^{2-} \leftrightarrow Yb(SO_4)_2^-$	5.10

In the first set of experiments (experiments 1 to 3 in Table 1), 11 species were presented, while in the second set of experiments (4 and 5 in table 1), 32 species were in solution. The huge number of variables to optimise represented a problem in terms of processing time. For that reason, the system was solved taking only the major components into account. With this approach, previously applied by Yaroshchuk et al. [32], the electric potential gradient is defined only by the major components, which allows the mathematical model to resolve trace ions one by one. This approach would allow the number of variables solved simultaneously to be reduced, and was translated into an improvement of the resolution time. Ion traces were considered those components whose concentration was less than 5% of the major components in solution.

4. Results and discussion

4.1. Recovery of sulphuric acid and rejection of dominant metal species

Figure 1 shows the rejection curves for the dominant electrolyte (H^+/SO_4^{2-}) in the presence of model metals (Al, Zn and Ca) as a function of transmembrane volume flow. Rejection was referred to the total component in solution regardless of its speciation, taking into account the values measured in solution for S, Al, Ca and Zn. The symbols represent the experimental points and the lines were derived by using the SDM equations (Eq. 1). Calculated membrane permeances to aqueous species are collected in Figure 2. In general, good agreement was obtained between experimental and modelled data for all of the dominant components (S, Al, Ca and Zn), except for the case of hydrogen ions (H^+), especially at higher pH values (1.9 and 2.5), resulting on an overestimation of its concentration. Rejection of sulphur at the maximum transmembrane flow decreased from 80% at the highest pH value evaluated (2.5) to 45% rejection at pH 1.0. This decrease was driven by: a) changes in speciation with pH, which resulted in the predominance of HSO_4^- at lower pH (<1.98) and of SO_4^{2-} at higher pH (>1.98); and by b) changes in the membrane acid-base properties, as free carboxylic and amine groups of the piperazine structure were protonated at lower pH, respectively, to R-COOH and $R_2NH_2^+$. NF270 isoelectric point (IEP) was determined experimentally, given a result of 3.4 ±0.1, which lies in between most of the published values of 2.8 to 3.5 [40].

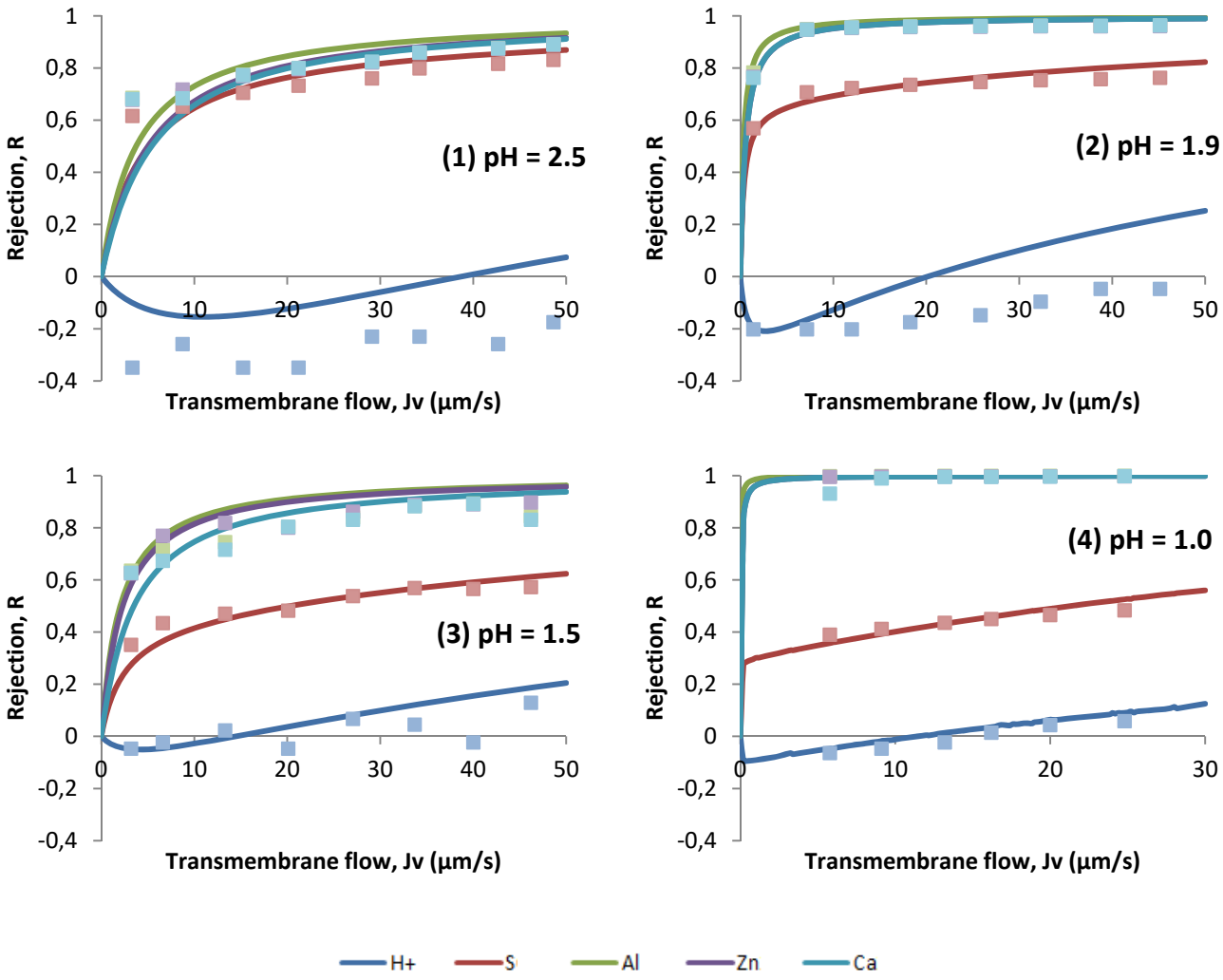

Figure 1. Rejection curves for the 1st set of experiments. Experiments were performed at cfv = 0.7 m/s. Solid lines represent the model prediction and the points the experimental data. (1) pH = 2.5; (2) pH = 1.9; (3) pH = 1.5; (4) pH = 1.0 . The membrane permeances used were those collected in Figure 2.

Although this characterisation technique does not provide information in terms of concentration of carboxylic (RCOOH/R-COO^-) and amine (R-NH_3^+/R-NH_2) groups or on the acidity constants of carboxylic groups, it can be assumed that for the experimental conditions used in this study (pH<2.5), the carboxylic groups were fully protonated (R-COOH). No information on the acid-base properties of the free membrane amines in the pH range evaluated in the IEP measurement (2 to 5) has been reported. Recently, Fernández et al. [41] have postulated potential piperazine groups and their theoretically calculated pK_a values. Accordingly, the acid-base membrane properties could be defined by eq. 5-6:

For the carboxylic groups: $P - COO^-B^+ + H^+HSO_4^- \leftrightarrow P - COOH + SO_4^{2-} + B^+$ (Eq. 5)

For the piperazine groups: $P - NR_2 + H^+HSO_4^- \leftrightarrow P - NR_2H^+HSO_4^-$ (Eq.6)

Where P represents the polyamide structure, COOH the carboxylic group, NR_2 the piperazine groups and B^+ represents an alkaline cation, typically K or Na from the solutions used during the polyamide polymerisation stage.

Navarro et al [23] evaluated the effect of acidic treatments (e.g. HF, H_3PO_4) onto polyamide-based NF membranes (DL) and found that for all of the membranes studied the IEPs corresponded to amphoteric surfaces. Given an

active surface of the PA layer, positive charges could be attributed to the protonation of the amine groups, while the negative zeta potential could be due to the dissociation of the carboxylic groups. The pre-treatments displaced the IEP towards lower pH values independent of the pre-treatment times.

Then, conditioning the membranes in acidic sulphuric solutions is accompanied by the protonation of the nitrogen atom of the piperazine groups, and the formation of an ionic pair with HSO_4^- major anion in the studied solutions. Analysis of FTIR (Figure S1.1 & S1.2 and Table S1.1, supplementary information) and XPS of virgin and aged membranes conditioned with sulphuric acid solutions, confirmed the presence of NH^+ (e.g. protonated amines) and OH^- (e.g. HSO_4^- and carboxylic acid groups) with a large band at 3400 cm^{-1} when virgin and aged membranes were compared. The FTIR spectra of the sulphuric aged NF270 membrane sample revealed a new band at 1468 cm^{-1}, which could be assigned to the stretching mode of HSO_4^-. The presence of HSO_4^- ions was also corroborated by the XPS spectra of the sulphuric aged sample with a band at 170 eV for S(2p). This band was not detected on the virgin N270. Table 3 collects the molar percentage of O, C, N and S for virgin and aged membrane. It can be seen that S/N molar ratio approaches to 1, indicating that most of the N atoms of the piperazine groups are protonated to the HSO_4^- form ($P\text{-}NR_2H^+HSO_4^-$). It should be remembered that piperazine groups contain two N atoms per molecule and only one terminal could be protonated.

Table 3. Atomic ratios and molar percentage of carbon, oxygen, nitrogen and sulphur in the membrane by XPS.

	% C	% O	% N	% S	C/O	O/N	S/O
Virgin membrane	72.5	16.8	10.7	-	4.3	1.6	-
Aged membrane	66.0	23.0	4.9	6.2	2.9	4.7	0.3

Under the acidic conditions in which the filtration experiments were conducted, the polyamide layer was equilibrated with sulphuric acid solutions. This favoured the transport of anions through the membrane and, thus, a decrease of the sulphuric rejection. Consequently, ion transport phenomena were controlled by the dominant electrolyte (H^+ SO_4^-) which drove the transport of other cationic species in solution to accomplish the electroneutrality condition. The membrane permeance to H^+ increased when pH was lowered and when sulphuric acid concentration increased, while the permeances for the double charged anions (SO_4^{2-} and $Zn(SO_4)_2^{2-}$) decreased with both influencing factors.

High metal rejections were obtained in accordance with the fact that feed solution pH was below the membrane IEP value, which resulted in a positively charged membrane, leading to higher cation rejections. Rejection values for Al, Ca and Zn increased from values around 75% at pH 2.5 up to values higher than 99% for pH 1. Although all these metals presented an oxidation state of +2 and +3 (Al, Ca and Zn), speciation analysis (Annex I) for the different synthetic solutions studied showed that these elements were mainly complexed, forming species with a single charge ($AlSO_4^+$, $CaHSO_4^+$), double charge ($Zn(SO_4)_2^{2-}$) and even with no charge ($CaSO_4$(aq) or $CuSO_4$ (aq)). This is of particular importance because ion rejection is mainly determined by Donnan exclusion and dielectric exclusion, which are strongly influenced by the membrane fixed charges and the ion charges [42]. Donnan exclusion is caused by charge interactions between ions in solution and the membrane surface. Dielectric exclusion is caused by the interaction between ions and the bound electric charges induced by ions at the interfaces in media of different dielectric constants (bulk solution/polymeric matrix). It was commonly believed that the main rejection mechanism was Donnan exclusion, which is caused by a fixed electric charge. However, Donnan exclusion could not explain the high rejection of multi-valent counter-ions, resulting in an underestimation of their values. Dielectric exclusion was postulated to improve the understanding of these rejections [42].

Of all of the ions in solution, and although the ionised membrane groups were expected to be protonated, the lower charged species such as H^+, $AlSO_4^+$ and $CaHSO_4^+$ were better transported according to the dielectric exclusion mechanism and driven by the need to achieve electroneutrality due to the transport of HSO_4^-. Proton (H^+) was the most favoured cation to permeate, because of its small size and its high concentration in such acidic stream compared with other cations in solution. Those with the higher absolute charge were more rejected according to the dielectric exclusion mechanism.

The reduction of pH led to a decrease in HSO_4^- rejection. This favoured the passage of H^+ through the membrane, resulting in negative rejection values, which in turn made the rejection of positively charged metal species higher.

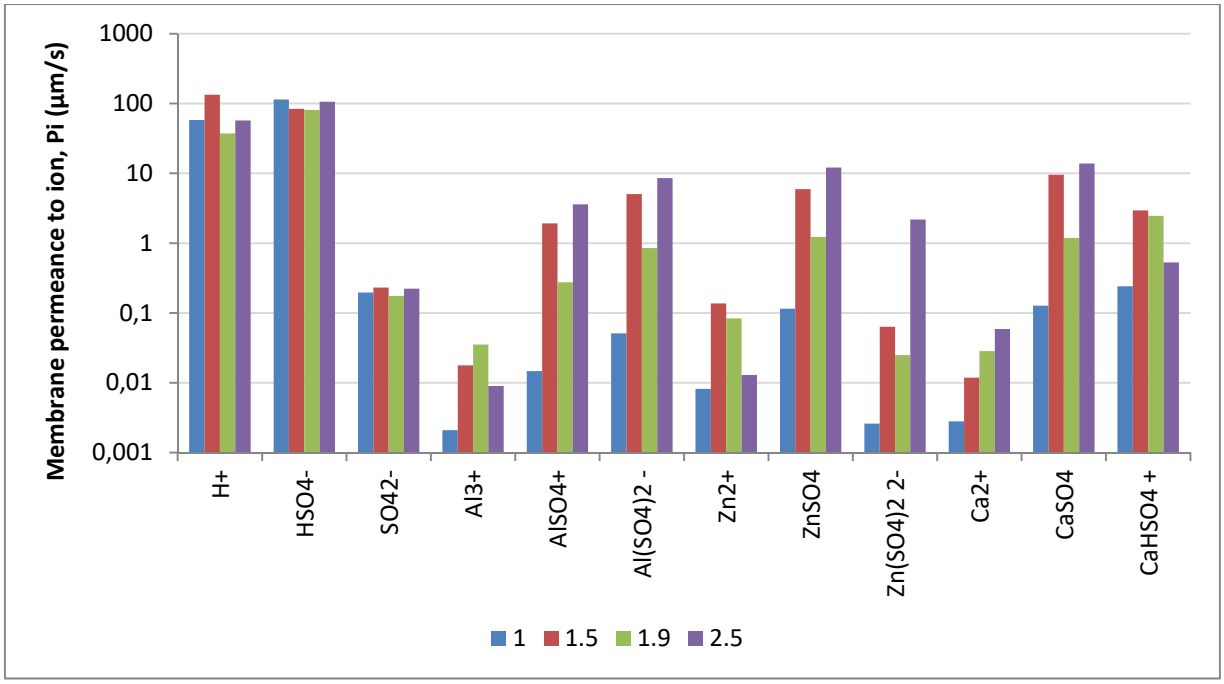

Figure 2. NF270 membrane permeances to major species, Pi (µm/s), for sulphuric solutions containing transition metallic ions (Ca, Zn and Al) at four different pH values.

Figure 2 collects the membrane permeance values obtained from the SDM and considering all the chemical species present in solution. The predicted values followed the expected trends, in which the permeance to an ion decreased as absolute value of the ion charge increased, e.g. single charged species $Al(SO_4)_2^-$ showed higher membrane permeances than double charged species (SO_4^{2-}, $Zn(SO_4)_2^{2-}$). Among the different mechanisms used to describe the separation in NF membrane, dielectric exclusion explained the obtained values [42].

From Figure 2 the contribution of each species to the global rejection of the major electrolytes (H_2SO_4, $Al_2(SO_4)_3$, $CaSO_4$, $ZnSO_4$) could be analysed. The most reactive species was SO_4^{2-} ion, which presented up to seven different forms in solution (SO_4^{2-}, HSO_4^-, $AlSO_4^+$, $Al(SO_4)_2^-$, $ZnSO_4$, $CaSO_4$ and $CaHSO_4^+$) followed by Al, Zn and Ca with three species in solution each. In general, permeances for most of the metal and metal-sulphate complexes had permeance values ranging from 100 to 1000 times lower (e.g, Al^{3+}, Ca^{2+} and Zn^{2+}) than the fastest ions (H^+, HSO_4^-). It is worth mentioning that non-charged complexes such as $ZnSO_4$(aq) and $CaSO_4$(aq) exhibited permeances values around one order of magnitude higher than those of charged species ($AlSO_4^+$, $Al(SO_4)_2^-$ and $CaHSO_4^+$).

It is reported that membrane permeances to both salt and ions are dependent on total electrolyte concentration [43]. In this study, values of permeance to single charge ions showed variations mostly lower than 10% over the ionic strength (IS) range evaluated (from $1.5x10^{-1}$ M at pH = 1 to $5x10^{-2}$ M at pH = 2.5), while permeance values to ions with higher charge decreased with the increase of IS. This strong decrease of permeance with the increase of

the electrolyte concentration was accompanied by a strong increase of the acidity, which modified the acid-base properties of the membrane and then affected the transport of cations across the membranes. At pHs lower than IEP, membrane exhibited a positive charge, and an electro-repulsion was produced between the polymer and the cations in solution, which became larger as the pH decreased. An opposite tendency was observed for the anions in solution. One main open question to be solved is the partitioning of non-charged species such as $CaSO_4$(aq) or $CuSO_4$ (aq). Such species are not expected to be influenced by electric fields and probably other mechanism should be evaluated.

Metal rejection results in sulphuric solutions were compared with published data using different NF membranes. Table S2.1 (supplementary information) sums up feed composition, pH, membrane properties and operation parameters. At low pH, sulphate rejection was found to be relatively low and increased when pH was also increased. For all cases, transition metal rejection was found to be high and independent of pH. Only Niewersch et al. [34] modelled ion rejections from sulphuric solutions originated from the dissolution of domestic sewage sludge incineration bottom ash using NF. Modelled ion rejection (for total P, Al, Mg and H^+) as a function of the permeate flux compared relatively well with the measured rejections. The strongest deviation was observed for the rejection of H^+ ions at higher permeate flux, for which the modelled rejection was, as in the present study, overestimated. As NF membranes used in their study and the present one had different chemical properties, comparison of membrane permeances to ions was not possible.

4.2. Rejection of REE metal species (La, Sm, Pr, Nd, Dy, Yb)

4.2.1 Virgin membrane

Figure 3 shows the rejection curves for the dominant electrolyte (H^+ SO_4^{2-}) in the presence of common metals (Al, Zn, Cu and Ca) and REEs (La, Sm, Pr, Nd, Dy, Yb) as a function of transmembrane volume flow (Experiment 4). Rejection is referred to the total concentration of the element regardless of speciation from the values measured in solution for S, Al, Ca, Cu, Zn and REE. The symbols represent the experimental points and the lines were derived by using the SDM equations (Eq. 1). Calculated membrane permeances to aqueous species are collected in Figure 4. A good prediction was obtained in the experiment carried out. The calculations were made by fitting the rejections of the dominant species and subsequently modelling the rejections of the trace/minor ions.

Sulphur rejection was quite low, due to the predominance of hydrogen sulphate (HSO_4^-) at pH = 1, and it increased from 35 to 50% as the trans-membrane flow increased. Metal ion rejections were found to be higher than 98% for all of the pressure range studied. Hydrogen rejection was low, starting from negative (-5%) to positive values (5%).

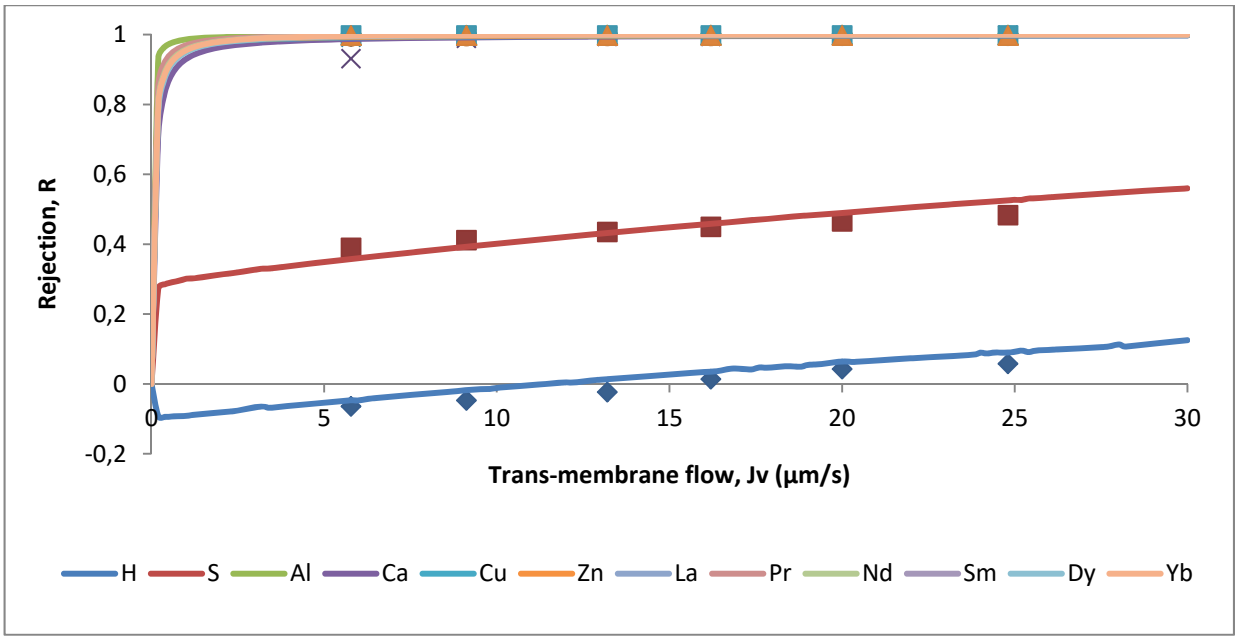

Figure 3. Rejection curves for NF270 in sulphuric solutions containing mixtures of transition metal ions and REEs at pH 1. Experiments were performed at pH = 1 and cfv = 0.7 m/s. Solid lines represent the model prediction using the SDM equations (Eq. 1) and the points the experimental data.

Similar trends were observed when the permeances for REE species were compared with those for the dominant elements in solution (Figure 4). REE elements were mainly present as triple charged species (M^{3+}) and as single charged species (MSO_4^+, $M(SO_4)_2^-$) and followed the expected behaviour defined by the dielectric exclusion mechanism for a polymeric NF membrane with a positively charged structure. Permeance values for M^{3+} species were between 1 to 2 orders of magnitude lower than those for the single charged species (MSO_4^+, $M(SO_4)_2^-$) and also lower than those determined for multi charged species for SO_4^{2-}, Al^{3+}, Ca^{2+}, Cu^{2+} and Zn^{2+}. When the membrane permeances to single charged cations were compared with those to single charged anions, it was found that the values of the latter were lower, in accordance with fact that membrane structure was positively charged.

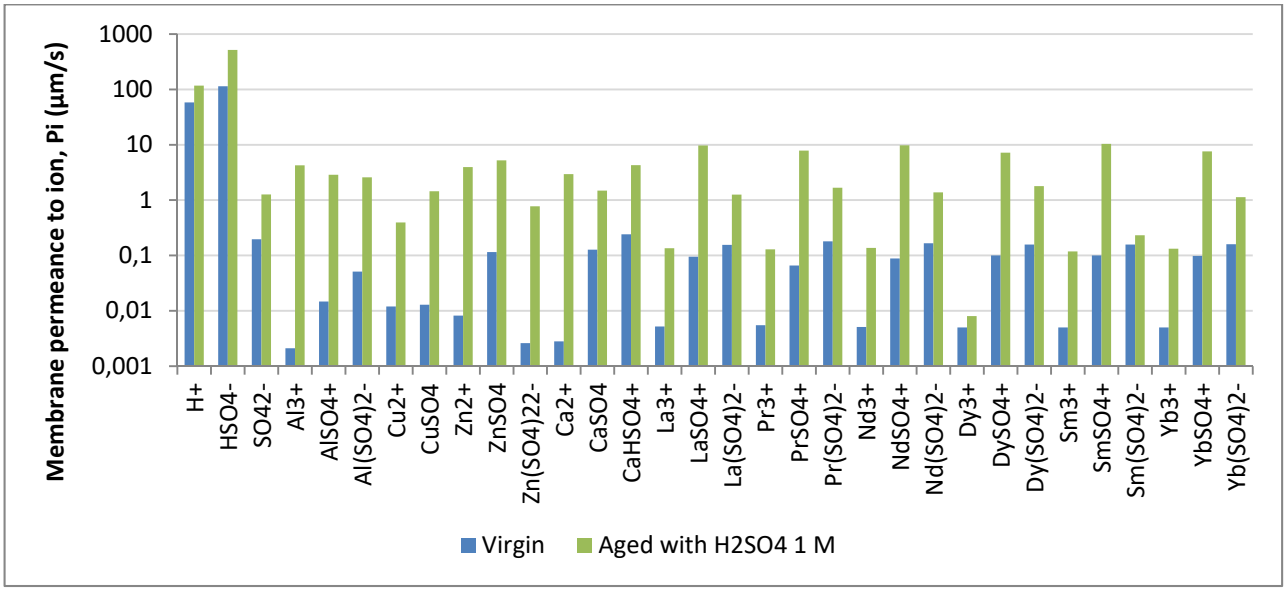

Figure 4. NF270 membrane permeance ion for the virgin and aged membrane (1 M sulphuric acid during 30 days) in sulphuric solution at pH =1. Experimental details are provided in table 2.

4.2.2. Aged membrane

Figure 5 shows the measured and predicted rejection curves for the NF270 membrane aged in 1 M sulphuric acid for one month. Points represents the experimental data and the solid lines the theoretical prediction. As previously mentioned, the system was solved with major components in solution (H^+, SO_4^{2-} and Al). Then, mathematical equations describing ion flux for traces (REE, Ca, Cu and Zn) were solved separately. Membrane permeances to ion are also presented in Figure 4.

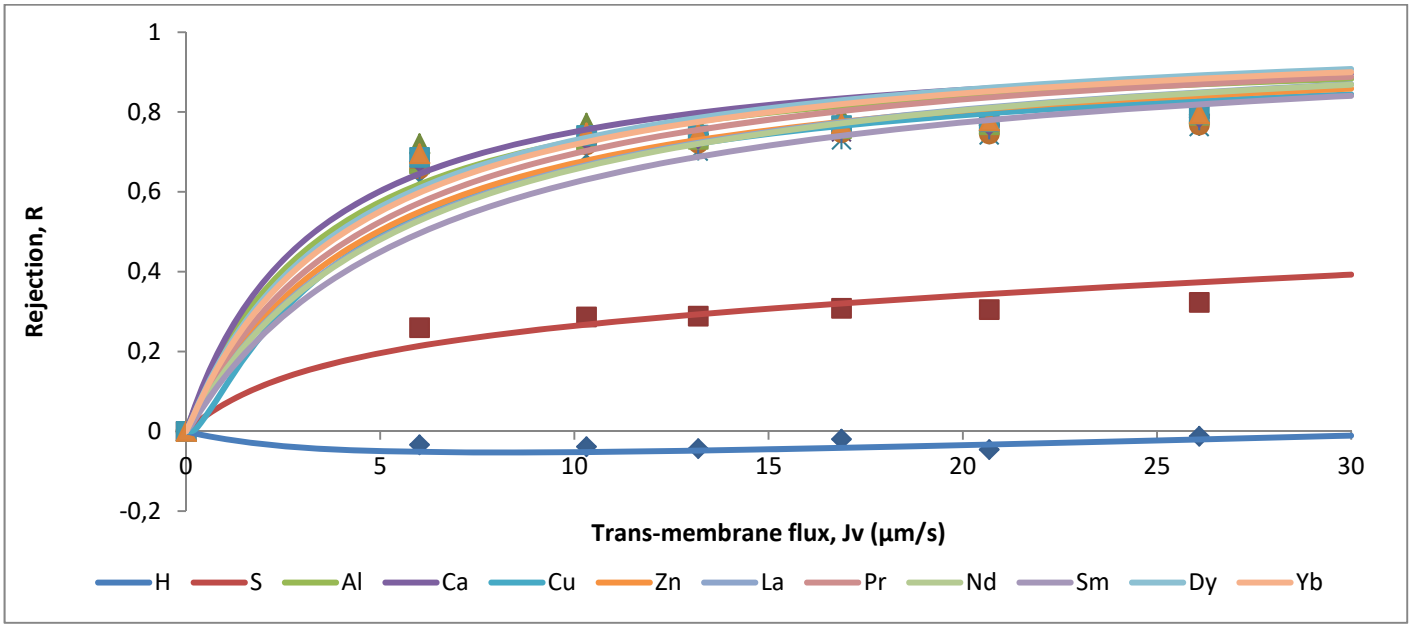

Figure 5. Rejection curves for aged NF270 in sulphuric solutions containing mixtures of transition metal ions and REEs at pH 1. Experiments were performed at pH = 1 and cfv = 0.7 m/s. Solid lines represent the model prediction and the point the experimental data.

Rejections of the major elements decreased from 99% to 70–80% for the metal species (Al, Ca, Cu and Zn) and slightly diminished for sulphur from 40 to 30%. These differences could be attributed to the fact that membrane aged in 1 M sulphuric acid suffered both physical and chemical modifications in such strong acidic conditions. Accordingly, these changes led to an equivalent increase in the membrane permeances to ions (Figure 4) for all of the species involved, e.g. between one and three orders of magnitude for multi-charged species, especially trivalent ions. For example, in the case of HSO_4^-, the permeance increased from 114 to 500 µm/s, and the same happened for the double-charged sulphate (from 0.2 to 1.3 µm/s). Membrane permeances for non-charged species have increased by a factor of 10 as minimum (e.g. $CaSO_4$). The differences became more significant in the case of trivalent species, e.g. permeance for free ion lanthanum increased from 0.001 to 0.135 µm/s.

Hydraulic permeability, at cfv of 1 m/s and a TMP=22 bar, increased from 3.4 ± 0.3 µm/s up to 4.0 ± 0.3 µm/s after ageing in 1 M sulphuric acid. Ricci et al. [44] reported an increase in water permeability of between 100 and 300% after four weeks of ageing using more diluted sulphuric acid solutions (e.g. 0.15 and 0.3 M) for a RO membrane based on polyamide and a NF membrane based on polysulphide and polyethersulphone. In contrast, Tanninen et al. [45] reported a decrease in water permeability from 36.4 to 17.5 µm/s (at a cfv of 2.5 m/s and a TMP = 15 bar) for NF270 with mixtures of copper sulphate and sulphuric acid. By assuming a pore flow model, in which a reduction in the values of reflection coefficients were considered after 8 weeks of exposure, it led to an increase of the solute convective flux caused by the increase of membrane pores sizes, resulting from its

degradation. However, no evidence was provided to confirm the effect of the acidity of the polyamide active layer structure.

The effect of exposure of the NF270 membrane to acidic conditions on its hydrophilicity was evaluated by determining the contact angle before and after four weeks of exposure. The virgin NF membrane presented a contact angle between 23°-32°, indicating a hydrophilic character [46–48]. The discrepancy between these angles can be attributed to differences in the operating conditions employed in each of the tests, such as the drop volume, temperature, humidity, and time measurements. After four weeks of immersion in sulphuric acid the contact angle rose to 23.2-53° (Figure S3.1, supplementary information). Ricci et al. [44], when evaluating the ageing of MPF-34 NF membrane with sulphuric solutions, reported the same behaviour, which was attributed to the degradation of the selective layer and exposure of the support layer with a greater hydrophobic character.

Chemical and physical changes of the piperazine-amide selective layer of NF270 were evaluated with XPS, FTIR and AFM. AFM surface images of 1x1 µm are shown in Figure 6. The light regions represent the highest points and the dark points are the depressions of the membrane. Contact mode AFM was used to obtain the roughness (RMS) prior and after four weeks to exposure to sulphuric solution. The virgin membrane surface appeared homogenous, while after four weeks of exposure to sulphuric acid, the emergence of scattered areas with changes in the selective layer and an increase in RMS roughness was noticed from 3.4 ± 0.2 nm to 1.9 ± 0.2 nm, indicating degradation of the selective layer and exposing the support layer. The small value of roughness was also reported by Fernández et al. [41], who concluded that the roughness of NF270 in comparison with a fully aromatic NF membrane NF90 was overtly lower as a consequence of the cross-linking degree of the monolayers that constitutes the membrane surface.

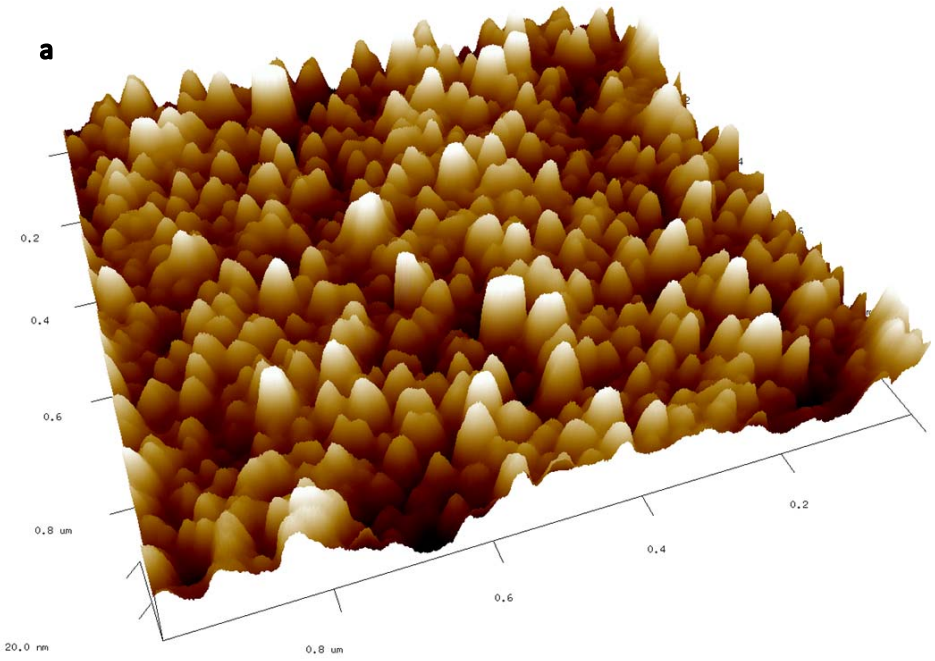

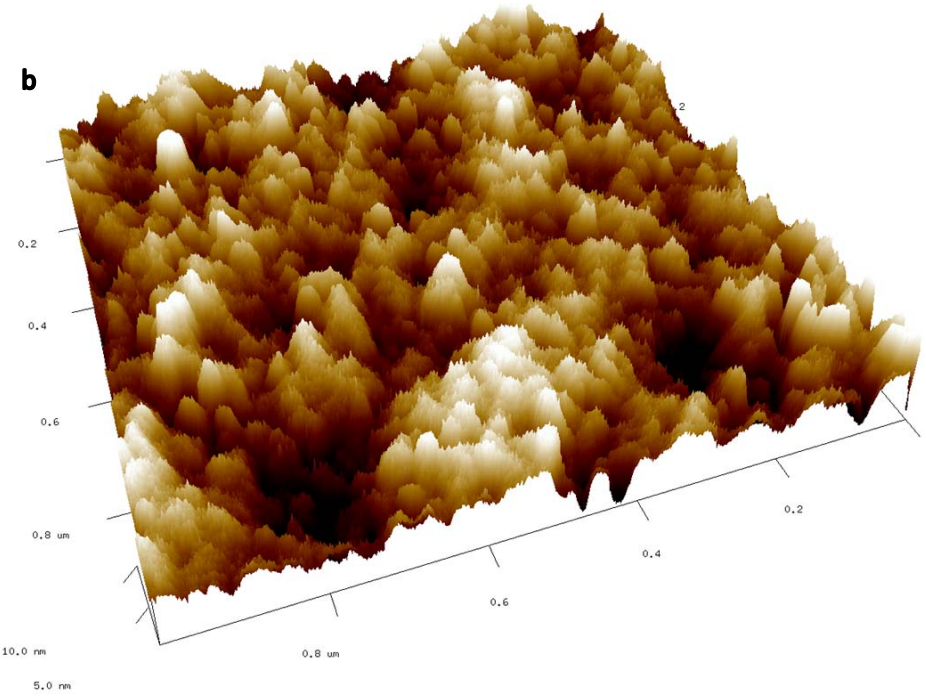

Figure 6. AFM images for NF-270 membrane; (a) Virgin, (b) Aged in1 M sulphuric acid

The effect of the exposure of the membrane to an acidic sulphuric solution on the chemical composition of the polyamide layer was also analysed by ATR-FTIR (Figures S1.1 & S1.2, supplementary information). The resulted spectra consisted of a superposition of the active (polyamide) and the intermediate layer (polysulphone), due to the fact that the radiation penetration depth was higher than the thickness of the active layer. Identification of the polymer bands of the active semi-aromatic polyamide layer is summarised in Table S1.1 (supplementary information) [49–56]. The main changes were associated to the protonation of the piperazine amine groups (NH^{2+}) and OH^- groups with a wide band at 3400 cm^{-1} and to the presence of HSO_4^- due to the appearance of three new bands (1468 cm^{-1} stretching band S=O; 1100 cm^{-1} OH stretching and 894.1 cm^{-1} S-O stretching) [56]. Navarro et al. [23], when analysing an aromatic polyamide based membrane (DSL) treated with HF and H_3PO_4, found that the relative relevance of the C=O bands (amide and acid) remained constant when compared with virgin samples. However, with H_3PO_4 solutions, there was an initial widening of the amide carbonyl band without changes in the relative intensity of C=O bands, and the amide carbonyl band was narrower and decreased when compared to the carboxylic group and different peaks linked to the polyamide also decreased suggesting a potential hydrolysis of the polyamide membrane groups. A potential mechanism was postulated, initiated by the protonation of the C=O group of the amide as described by Eq. 7

$$\text{-(R--NH-(C=O)—R)}_n\text{-- } + H^+X^- \leftrightarrow \text{-(R--NH-(C=O)}H^+X^-\text{ --R)}_n\text{--} \quad \text{(where } X^- \text{ is the strong electrolyte } (HSO_4^-)\text{)} \quad \text{Eq. 7}$$

XPS analysis confirmed the presence of sulphate in the acidic aged samples. Then, in a second step, the hydrolysis of the C=O promoted the formation of free amine and carboxylic groups on the structure. The reduction in cross-linking of the polyamide layer could lead to an increase in the free-volume size. As dielectric exclusion from the polymer network pores of the membranes with closed geometry is shown to be essentially stronger than that from free volume with relatively open geometry [57], the modification of the PA seemed to weaken the screening mechanism resulting in an increase of permeances to ions for all the species.

XPS results showed the presence of carbon, oxygen and nitrogen in both membranes, in addition to the presence of sulphur in the aged membrane, as shown in Table S4.1 (supplementary information). Peaks were centred in

170 eV for S(2p), 284.9 eV for C(1s), 399 for N(1s) and 531 eV for O(1s). Hydrogen was not included in the list above, due to the unsuitability of XPS for its analysis. Table 3 collects the ratios between the different elements.

Oxygen atomic ratio (O/N) lay between 1 and 2. In a fully cross-linked polyamide, each oxygen is bound to a nitrogen atom in an amide bond (O/N of 1) while in a fully linear polyamide (O/N ratio of 2), as there are additional oxygen atoms in the free carboxylic groups [51]. The higher ratio of O/N and lower of C/O of aged membrane suggested a certain hydrolysis of the polyamide chain due to a higher degree of free carboxylic groups. The appearance of sulphur in the active layer is also noticeable. The presence of sulphate in the membrane could be explained by a partial hydrolysis or protonation of the N atoms of the piperazine groups. Additional information of the structure changes was obtained by analysis by deconvolution of the main element peaks shown in Table S4.1 (supplementary information); while Table S4.2 (supplementary information) summarises the peak assignment and their contribution to the total peak surface area.

For the virgin membrane, three peaks were identified for C (1s): at 284.6 eV, which was associated to C-C, C-H and C=C chemical bindings; at 285.8 eV which was related to C-O and C-N chemical bindings; and at 287.56 eV, associated to C=O-N, N=C and C=O chemical bindings; [47,51,58]. The aged membrane showed the presence of new peaks at 291.4 and 292.7 eV associated to π - π bonds. For nitrogen, two peaks were found at 399.9 and 401.5 eV, which were associated to C-N, C=N, O=C-N and to $-NH_3^+$, $-NH_2R^+$ chemical bindings, respectively. In relation to the proportion of these types of nitrogen binding, the contribution for the first one was around 95% and 5% for the other one. Their contribution, however, changed for the aged sample. The component at 399.9 eV for N(1s) decreased down to 52% of total nitrogen peak intensity, which meant a strong increase of the NH_3^+ groups. Similar results have been reported by Stevens et al. [59] when analysing complex amino acids and by Amaral et al. [60] when chitosan was modified by phosphorylation. The upward shift of the electron bonding energy of the peaks associated to protonated amine groups of the piperazine structure has also been reported by FTIR analysis.

For oxygen, O(1s) levels are rather broad in nature (2 eV) and two peaks were identified at 531.2 eV, which was associated to O=C-N, C=O, C-O chemical bindings, and at 532.8 eV associated to H···O=C-N, O=C-O, C-OH chemical bindings [47]. For the aged membrane, one additional peak was observed at 531.6 eV, which was related to SO_4^{2-} [61]. Amaral et al. [60] associated this peak to a) physio-sorbed water associated to HSO_4^- or b) HSO_4^- bonds to protonated amine groups. Additionally, an increase of the contribution of the peak at 532 eV associated to oxygen atom on carboxylic protonated groups was observed from 24 to 64 %. It could be observed that for C (1s) there was a decrease in the area of the peak related to C=O-N, N=C, C=O chemical bindings; consequently, there was an increase in the two other two. This suggests that the membrane had suffered partial hydrolysis, which led to an increase of carboxylic and amine groups. The same conclusion could be achieved when the percentage of bonds for O (1s) and N (1s) were compared. In the case of oxygen, the percentage of the peak related to O=C-N decreased while the one related to carboxylic group increased. Finally, for nitrogen a decrease of amide groups was observed.

5. Conclusions

The treatment of free iron AMD streams with a semi-aromatic piperazine amide-based NF membrane (NF270) provided in an effective way to recover sulphuric and to concentrate metals. The high rejections for metal obtained make NF an attractive technology to be combined with other procedures to recover REE metals such as ion exchange resins. The membrane properties in such acidic media (1 to 2.5) was able to strongly change the performance in neutral solutions as the free carboxylic and piperazine groups were fully protonated and acid-base

properties changed. Transport of anionic species was favoured, as the membrane groups ionised were positively charged, and as a consequence the major ion in solution (HSO_4^-) was highly transported favouring the recovery of sulphuric acid. Although the complex nature of the treated solutions, in terms of reactivity where metal and non-metals species were forming a large number of complexes, its reactive transport was well described by using the SDM. Membrane permeances to ions for the different species were determined and their values reflected membrane properties. Ion transport seemed to be strongly controlled by the dielectric exclusion mechanisms and ions with the higher charges (positive or negative) were well strongly rejected. In very narrow pores, dielectric exclusion might be very strong, leading to a major screening and, then, to a separation improvement. However, it should be reminded that in fine pores with electric walls, the electrostatic interactions between fixed charges and counter-ions were essentially stronger than in aqueous solution. Accordingly, the degree of dissociation of ionised groups (e.g. amine and carboxylic) and the effective fixed charge density might be much smaller than those expected from the acid-base groups dissociation constant values. A finite degree of dissociation of ionized groups made the interference between dielectric and Donnan exclusion a more complex phenomenon. To be able to quantify the relative contributions of dielectric and Donnan exclusion a more detailed and complete characterisation of membrane transport properties need to be performed.

Membrane stability in acidic solutions was accelerated by ageing one membrane in 1 M sulphuric acid for 30 days. Chemical changes quantified by XPS and FTIR and contact angle indicated a partial hydrolysis of the amide groups that entailed in a potential increase of permanent ionised groups, increasing the size of the free pore volumes and consequently reducing the sieving mechanism controlled by the dielectric exclusion. Metal ion rejection, even triple charged ions of Al and REE, and also double charged ions decreased from 99% to 70% while the transport of the major electrolyte (H^+/SO_4^{2-}) was slightly increased. Changes in the membrane have enhanced ion transport and, as a consequence, the membrane permeance to ions. From the point of view of recovering strong acids (e.g. sulphuric acid) the membrane performance was improved by its ageing in an acidic media. However, if the objective is the rejection of metallic species, this target could be damaged by continuous acid exposure. Membrane attack would decrease the rejection of metallic ions, and a portion of REE and transition metals would be lost from the concentrate stream. Therefore, more stable membranes must be employed. In order to improve the membrane performance under continuous operation, it is necessary to perform a stability test of the membrane towards the specific solution to which it will be exposed. Values of membrane permeance to ions would give a measurement of the membrane stability and they could be a solution to control membrane performance.

Nomenclature

a^*	Debye Hückel parameter
c_i	Concentration of component i inside the membrane
C_{ip}	Concentration of component i in permeate side
IS	Ionic strength
j_i	Ion flux
J_v	Solvent trans-membrane flux
K	Equilibrium constant
P_i	Membrane permeance to ion i
x	Dimensionless position in the membrane
z_i	Ion charge
φ	Dimensionless electric potential in the membrane
γ_i	Activity coefficient

Acknowledgments

This research was supported by the CTM2014-57302-R, CGL2016-78783-C2-02, CTM2014-61221-JIN and ERAMIN-PCIN2015-242-256 projects financed by the Spanish Ministerio de Economía y Competitividad (MINECO) and by the Catalan Government (Project Ref. 2014SGR50). The work of Julio López was supported by the Spanish Ministry (MINECO) within the scope of the grant BES-2015-075051. The authors wish to thank Dow Chemical for the supply of the membranes, M. Cabañas, R. Bartrolí and J. Bellés (IDAEA-CSIC) for their analytical assistance and A. Yaroshchuk for his valuable contribution to the work.

Annex I – Speciation diagrams

Hydrogen

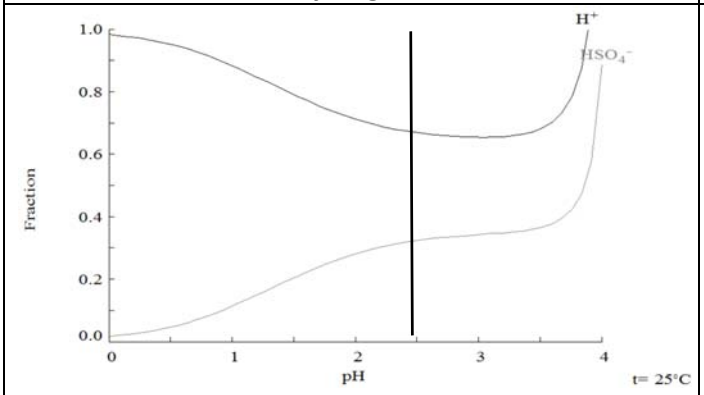

Sulphate

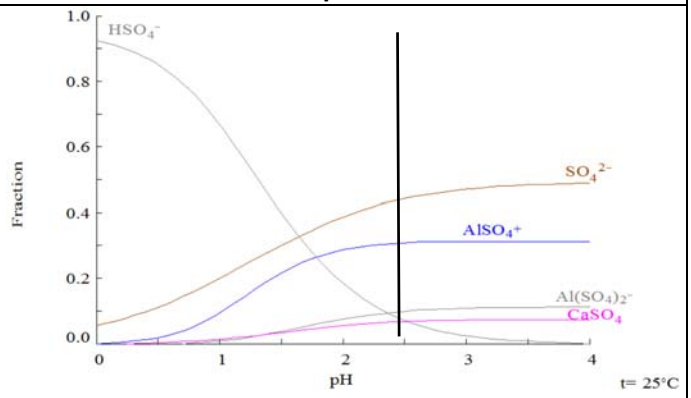

Aluminium

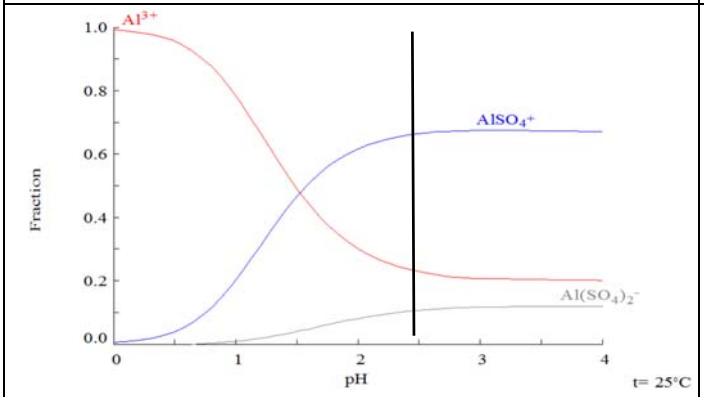

Calcium

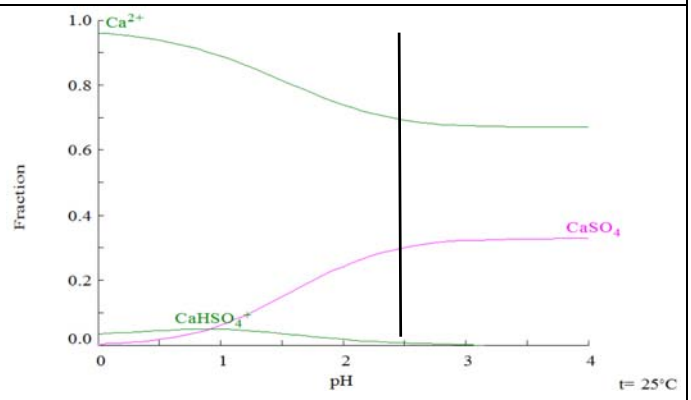

Zinc

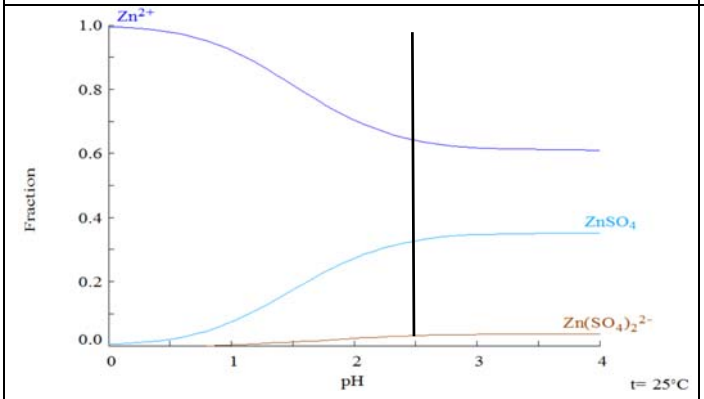

pH = 2.5

Hydrogen	Sulphate
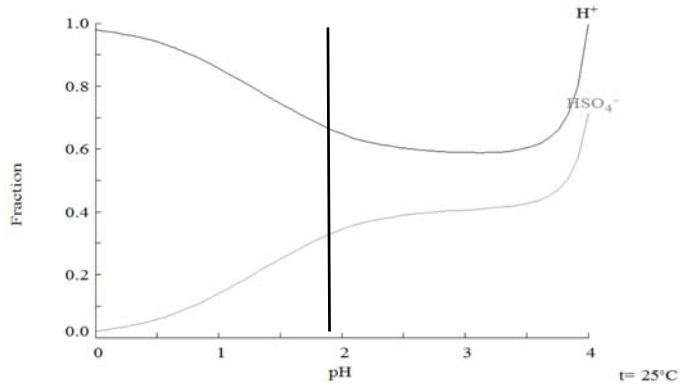	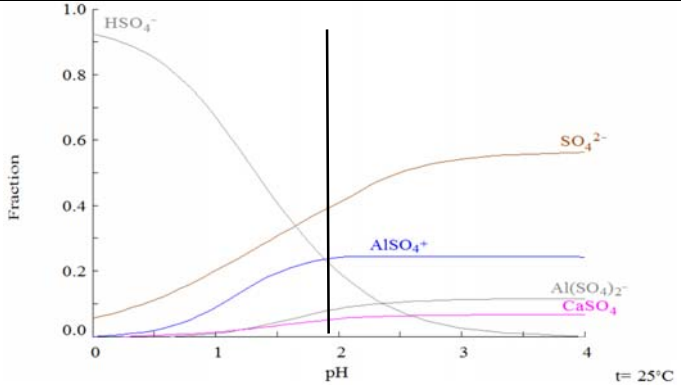
Aluminium	**Calcium**
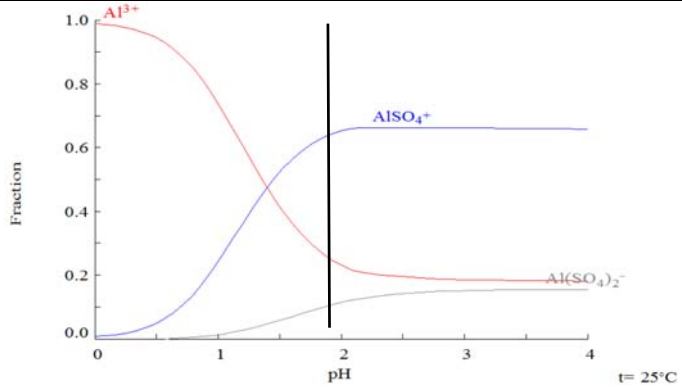	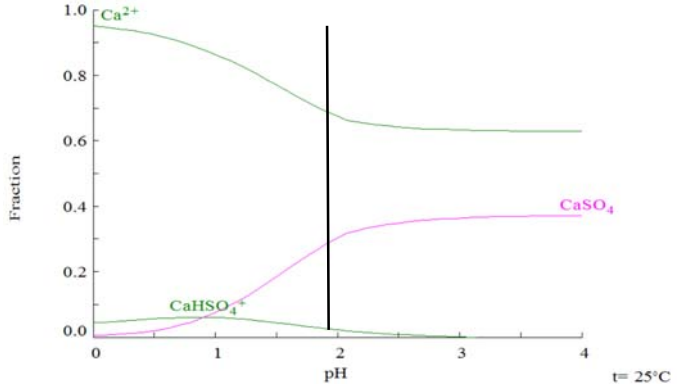
Zinc	
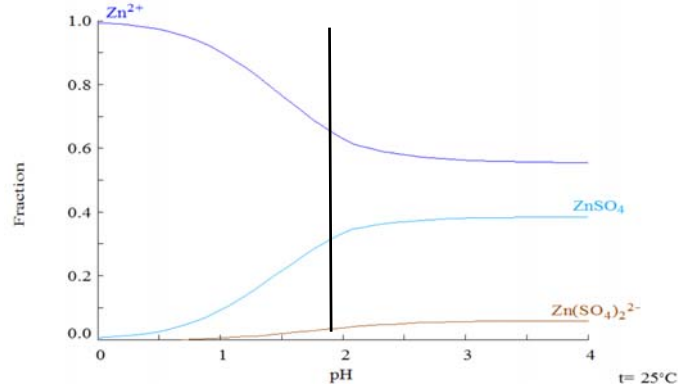	pH = 1.9

Hydrogen	Sulphate
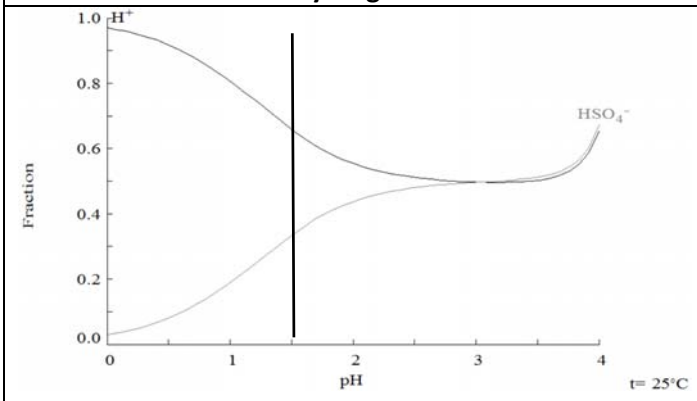	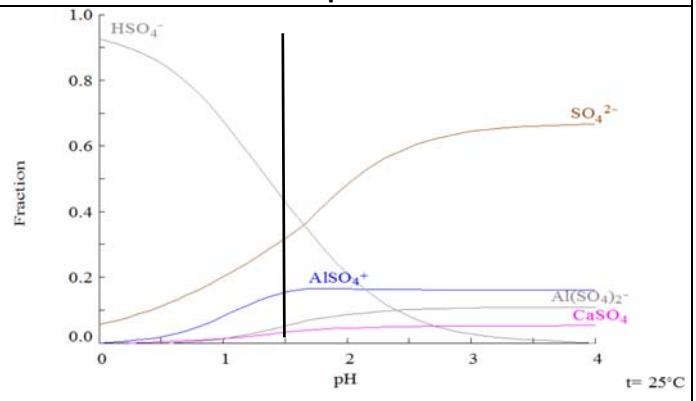
Aluminium	**Calcium**
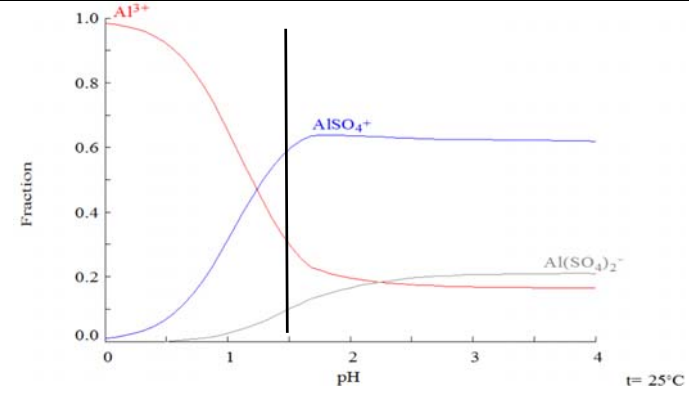	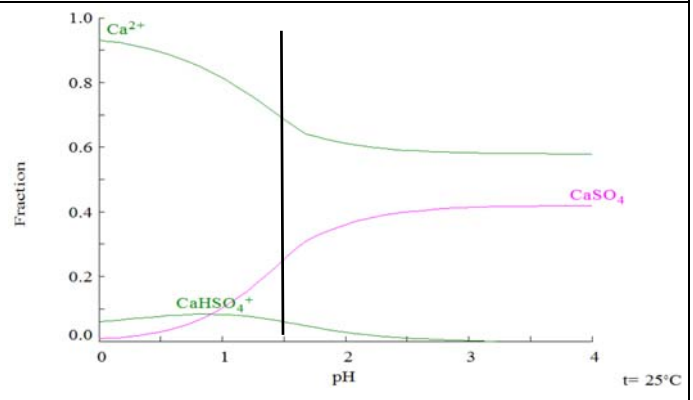
Zinc	
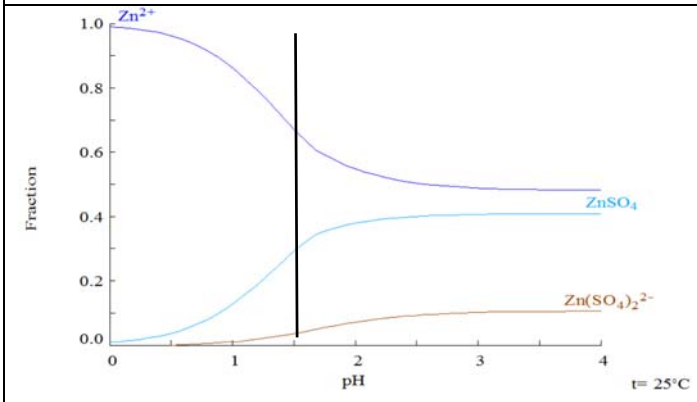	pH = 1.5

Hydrogen	Sulphate
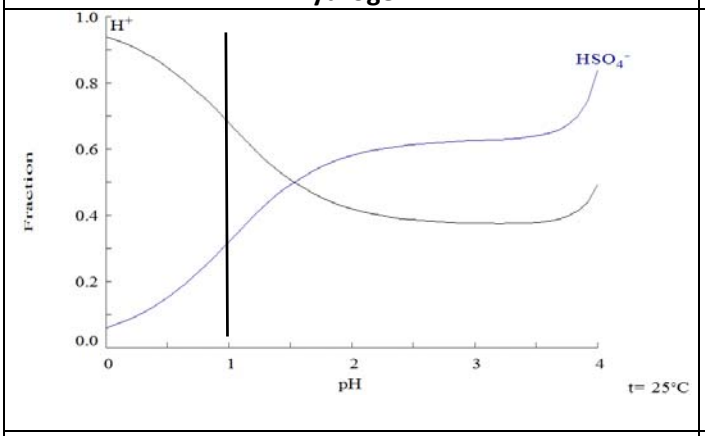	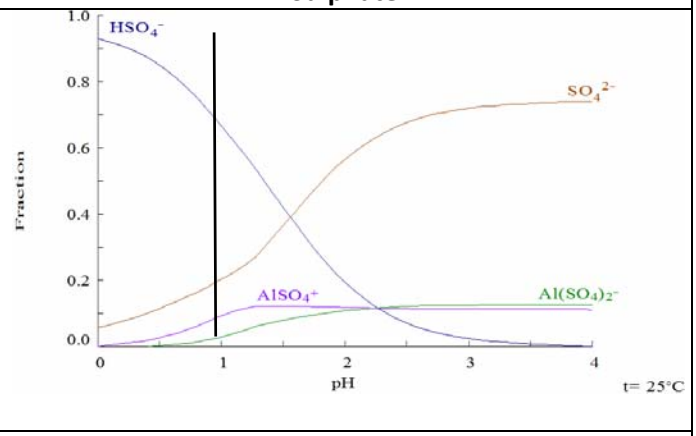
Aluminium	**Calcium**
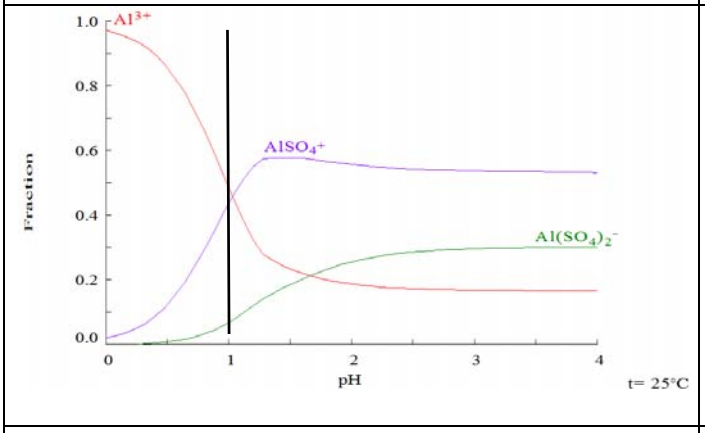	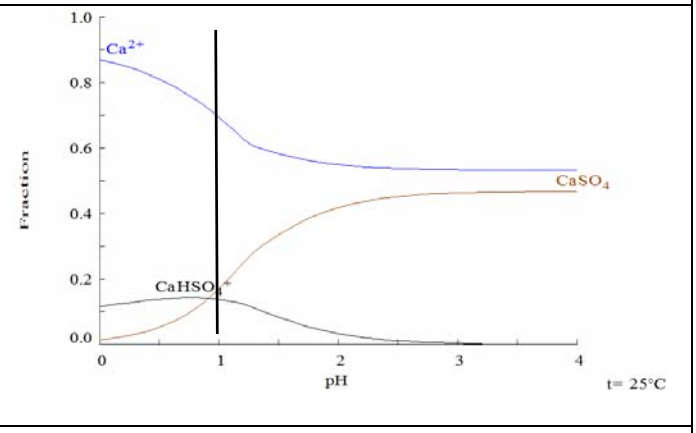
Zinc	**Copper**
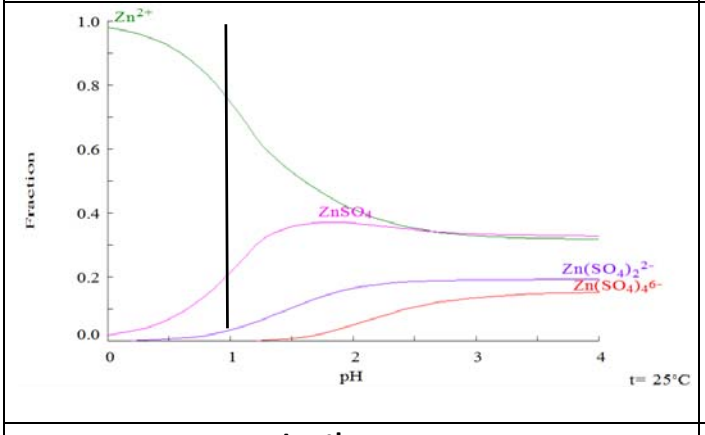	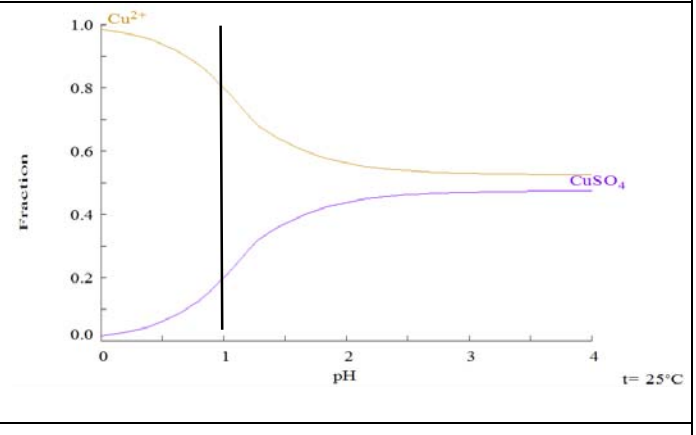
Lanthanum	
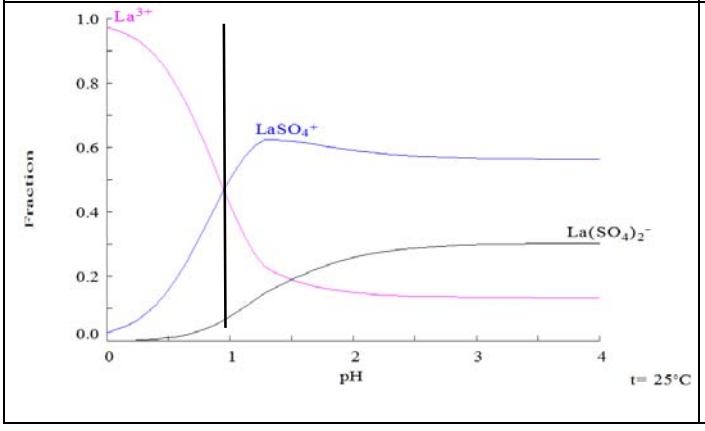	pH = 1.0

References

[1] G.S. Simate, S. Ndlovu, Acid mine drainage: Challenges and opportunities, J. Environ. Chem. Eng. 2 (2014) 1785–1803. doi:10.1016/j.jece.2014.07.021.

[2] S.M. MacLennan, Rare Earth Elements in sedimentary rocks: Influence of provenance and sedimentary processes., B.R. Lipin G.A. McKay "Geochemistry Mineral. Rare Earth Elem. Rev. Mineral. (1989) 169–200.

[3] C.W. Noack, D.A. Dzombak, A.K. Karamalidis, Rare Earth Element Distributions and Trends in Natural Waters with a Focus on Groundwater, Environ. Sci. Technol. 48 (2014) 4317–4326. doi:10.1021/es4053895.

[4] C. Ayora, F. Macías, E. Torres, A. Lozano, S. Carrero, J.M. Nieto, R. Pérez-López, A. Fernández-Martínez, H. Castillo-Michel, Recovery of Rare Earth Elements and Yttrium from Passive-Remediation Systems of Acid Mine Drainage, Environ. Sci. Technol. 50 (2016) 8255–8262. doi:10.1021/acs.est.6b02084.

[5] J. Sánchez España, E. López Pamo, E. Santofimia, O. Aduvire, J. Reyes, D. Barettino, Acid mine drainage in the Iberian Pyrite Belt (Odiel river watershed, Huelva, SW Spain): Geochemistry, mineralogy and environmental implications, Appl. Geochemistry. 20 (2005) 1320–1356. doi:10.1016/j.apgeochem.2005.01.011.

[6] M. Olías, C.R. Cánovas, J.M. Nieto, A.M. Sarmiento, Evaluation of the dissolved contaminant load transported by the Tinto and Odiel rivers (South West Spain), Appl. Geochemistry. 21 (2006) 1733–1749. doi:10.1016/j.apgeochem.2006.05.009.

[7] C. Ayora, M.A. Caraballo, F. Macias, T.S. Rötting, J. Carrera, J.-M. Nieto, Acid mine drainage in the Iberian Pyrite Belt: 2. Lessons learned from recent passive remediation experiences, Environ. Sci. Pollut. Res. 20 (2013) 7837–7853. doi:10.1007/s11356-013-1479-2.

[8] A.L. Mackie, M.E. Walsh, Bench-scale study of active mine water treatment using cement kiln dust (CKD) as a neutralization agent, Water Res. 46 (2012) 327–334. doi:10.1016/j.watres.2011.10.030.

[9] O. Gibert, J. de Pablo, J.L. Cortina, C. Ayora, Treatment of acid mine drainage by sulphate-reducing bacteria using permeable reactive barriers: A review from laboratory to full-scale experiments, Rev. Environ. Sci. Biotechnol. 1 (2002) 327–333. doi:10.1023/A:1023227616422.

[10] C.-M. Neculita, G.J. Zagury, B. Bussière, Passive Treatment of Acid Mine Drainage in Bioreactors using Sulfate-Reducing Bacteria: Critical review and research needs, J. Environ. Qual. 36 (2007) 1–16. doi:10.2134/jeq2006.0066.

[11] T. Ogata, H. Narita, M. Tanaka, Adsorption behavior of rare earth elements on silica gel modified with diglycol amic acid, Hydrometallurgy. 152 (2015) 178–182. doi:10.1016/j.hydromet.2015.01.005.

[12] K. Kondo, T. Matsuo, M. Matsumoto, Adsorptive separation of La, Ce and Pr using microcapsules containing 2-ethylhexylphosphonic acid mono-2-ethylhexyl ester, Hydrometallurgy. 152 (2015) 204–213. doi:10.1016/j.hydromet.2015.01.004.

[13] L. Cifuentes, I. García, P. Arriagada, J.M. Casas, The use of electrodialysis for metal separation and water recovery from CuSO4-H2SO4-Fe solutions, Sep. Purif. Technol. 68 (2009) 105–108. doi:10.1016/j.seppur.2009.04.017.

[14] L. Cifuentes, M. Grágeda, G. Crisóstomo, Electrowinning of copper in two- and three-compartment reactive electrodialysis cells, Chem. Eng. Sci. 61 (2006) 3623–3631. doi:10.1016/j.ces.2006.01.008.

[15] C.-M. Zhong, Z.-L. Xu, X.-H. Fang, L. Cheng, Treatment of Acid Mine Drainage (AMD) by Ultra-Low-Pressure

Reverse Osmosis and Nanofiltration, Environ. Eng. Sci. 24 (2007) 1297–1306. doi:10.1089/ees.2006.0245.

[16] H. Al-Zoubi, A. Rieger, P. Steinberger, W. Pelz, R. Haseneder, G. Härtel, Nanofiltration of Acid Mine Drainage, Desalin. Water Treat. 21 (2010) 148–161. doi:10.5004/dwt.2010.1316.

[17] H. Al-Zoubi, A. Rieger, P. Steinberger, W. Pelz, R. Haseneder, G. Härtel, Optimization Study for Treatment of Acid Mine Drainage Using Membrane Technology, Sep. Sci. Technol. 45 (2010) 2004–2016. doi:10.1080/01496395.2010.480963.

[18] M. Mullett, R. Fornarelli, D. Ralph, Nanofiltration of mine water: impact of feed pH and membrane charge on resource recovery and water discharge, Membranes (Basel). 4 (2014) 163–180. doi:10.3390/membranes4020163.

[19] R. Fornarelli, M. Mullett, D. Ralph, Factors influencing nanofiltration of acid mine drainage, Reliab. Mine Water Technol. (2013) 563–568.

[20] T.J.K. Visser, S.J. Modise, H.M. Krieg, K. Keizer, The removal of acid sulphate pollution by nanofiltration, Desalination. 140 (2001) 79–86.

[21] S. Platt, M. Nyström, A. Bottino, G. Capannelli, Stability of NF membranes under extreme acidic conditions, J. Memb. Sci. 239 (2004) 91–103. doi:10.1016/j.memsci.2003.09.030.

[22] A. Manis, K. Soldenhoff, E. Jusuf, F. Lucien, Separation of copper from sulfuric acid by nanofiltration, in: Fifth Int. Membr. Sci. Technol. Conf., 2003.

[23] R. Navarro, M.P. González, I. Saucedo, M. Avila, P. Prádanos, F. Martínez, A. Martín, A. Hernández, Effect of an acidic treatment on the chemical and charge properties of a nanofiltration membrane, J. Memb. Sci. 307 (2008) 136–148. doi:10.1016/j.memsci.2007.09.015.

[24] H. Diallo, M. Rabiller-Baudry, K. Khaless, B. Chaufer, On the electrostatic interactions in the transfer mechanisms of iron during nanofiltration in high concentrated phosphoric acid, J. Memb. Sci. 427 (2013) 37–47. doi:10.1016/j.memsci.2012.08.047.

[25] J. Tanninen, S. Platt, M. Nyström, Nanofiltration of sulphuric acid from metal sulphate solutions, Proc. Imstec 2003, Sydney. (n.d.) 1–6.

[26] E. Idil Mouhoumed, A. Szymczyk, A. Schäfer, L. Paugam, Y.H. La, Physico-chemical characterization of polyamide NF/RO membranes: Insight from streaming current measurements, J. Memb. Sci. 461 (2014) 130–138. doi:10.1016/j.memsci.2014.03.025.

[27] W.J. Koros, G.K. Fleming, S.M. Jordan, T.H. Kim, H.H. Hoehn, Polymeric membrane materials for solution-diffusion based permeation separations, Prog. Polym. Sci. 13 (1988) 339–401. doi:10.1016/0079-6700(88)90002-0.

[28] N. Pagès, M. Reig, O. Gibert, J.L. Cortina, Trace ions rejection tunning in NF by selecting solution composition: Ion permeances estimation, Chem. Eng. J. 308 (2017) 126–134. doi:10.1016/j.cej.2016.09.037.

[29] A. Yaroshchuk, T. Luxbacher, Interpretation of electrokinetic measurements with porous films: Role of electric conductance and streaming current within porous structure, Langmuir. 26 (2010) 10882–10889. doi:10.1021/la100777z.

[30] A. Yaroshchuk, X. Martínez-Lladó, L. Llenas, M. Rovira, J. de Pablo, J. Flores, P. Rubio, Mechanisms of transfer of ionic solutes through composite polymer nano-filtration membranes in view of their high sulfate/chloride selectivities, Desalin. Water Treat. 6 (2009) 48–53.

[31] A. Yaroshchuk, M.L. Bruening, E.E. Licón Bernal, Solution-Diffusion-Electro-Migration model and its uses

for analysis of nanofiltration, pressure-retarded osmosis and forward osmosis in multi-ionic solutions, J. Memb. Sci. 447 (2013) 463–476. doi:10.1016/j.memsci.2013.07.047.

[32] A. Yaroshchuk, X. Martínez-Lladó, L. Llenas, M. Rovira, J. de Pablo, Solution-diffusion-film model for the description of pressure-driven trans-membrane transfer of electrolyte mixtures: One dominant salt and trace ions, J. Memb. Sci. 368 (2011) 192–201. doi:10.1016/j.memsci.2010.11.037.

[33] N. Pages, A. Yaroshchuk, O. Gibert, J.L. Cortina, Rejection of trace ionic solutes in nanofiltration : Influence of aqueous phase composition, Chem. Eng. Sci. 104 (2013) 1107–1115. doi:10.1016/j.ces.2013.09.042.

[34] C. Niewersch, A.L.B. Bloch, S. Yüce, T. Melin, M. Wessling, Nanofiltration for the recovery of phosphorus — Development of a mass transport model, Desalination. 346 (2014) 70–78. doi:10.1016/j.desal.2014.05.011.

[35] C. Niewersch, Nanofiltration for phosphorus recycling from sewage sludge, Verlagshaus Mainz GmbH, 2013.

[36] O. Kedem, V. Freger, Determination of concentration-dependent transport coefficients in nanofiltration : Defining an optimal set of coefficients, J. Memb. Sci. 310 (2008) 586–593. doi:10.1016/j.memsci.2007.11.045.

[37] S. Bason, O. Kedem, V. Freger, Determination of concentration-dependent transport coefficients in nanofiltration : Experimental evaluation of coefficients, J. Memb. Sci. 326 (2009) 197–204. doi:10.1016/j.memsci.2008.09.054.

[38] S. Bason, Y. Kaufman, V. Freger, Analysis of Ion Transport in Nanofiltration Using Phenomenological Coefficients and Structural Characteristics, J. Phys. Chem B. 114 (2010) 3510–3517.

[39] I. Puigdomenech, Chemical equilibirum software Hydra/Medusa, (2001). https://sites.google.com/site/chemdiagr/home.

[40] G. Artuğ, I. Roosmasari, K. Richau, J. Hapke, A Comprehensive Characterization of Commercial Nanofiltration Membranes, Sep. Sci. Technol. 42 (2007) 2947–2986. doi:10.1080/01496390701560082.

[41] J.F. Fernández, B. Jastorff, R. Störmann, S. Stolte, J. Thöming, Thinking in terms of structure-activity-relationships (T-SAR): A tool to better understand nanofiltration membranes, Membranes (Basel). 1 (2011) 162–183. doi:10.3390/membranes1030162.

[42] A.E. Yaroshchuk, Dielectric exclusion of ions from membranes, Adv. Colloid Interface Sci. 85 (2000) 193–230. doi:10.1016/S0001-8686(99)00021-4.

[43] M. Reig, E. Licon, O. Gibert, A. Yaroshchuk, J.L. Cortina, Rejection of ammonium and nitrate from sodium chloride solutions by nanofiltration: Effect of dominant-salt concentration on the trace-ion rejection, Chem. Eng. J. 303 (2016) 401–408. doi:10.1016/j.cej.2016.06.025.

[44] B.C. Ricci, C.D. Ferreira, L.S. Marques, S.S. Martins, B.G. Reis, M.C.S. Amaral, Assessment of the chemical stability of nanofiltration and reverse osmosis membranes employed in treatment of acid gold mining effluent, Sep. Purif. Technol. 174 (2017) 301–311. doi:10.1016/j.seppur.2016.11.007.

[45] J. Tanninen, M. Mänttäri, M. Nyström, Effect of electrolyte strength on acid separation with NF membranes, J. Memb. Sci. 294 (2007) 207–212. doi:10.1016/j.memsci.2007.02.042.

[46] J. Tanninen, S. Platt, A. Weis, M. Nyström, Long-term acid resistance and selectivity of NF membranes in very acidic conditions, J. Memb. Sci. 240 (2004) 11–18. doi:10.1016/j.memsci.2004.04.006.

[47] V.T. Do, C.Y. Tang, M. Reinhard, J.O. Leckie, Degradation of polyamide nanofiltration and reverse osmosis membranes by hypochlorite, Environ. Sci. Technol. 46 (2012) 852–859. doi:10.1021/es203090y.

[48] D.J. Johnson, S.A. Al Malek, B.A.M. Al-Rashdi, N. Hilal, Atomic force microscopy of nanofiltration membranes: Effect of imaging mode and environment, J. Memb. Sci. 389 (2012) 486–498. doi:10.1016/j.memsci.2011.11.023.

[49] V. Freger, J. Gilron, S. Belfer, TFC polyamide membranes modified by grafting of hydrophilic polymers: An FT-IR/AFM/TEM study, J. Memb. Sci. 209 (2002) 283–292. doi:10.1016/S0376-7388(02)00356-3.

[50] M. Kallioinen, T. Sainio, J. Lahti, A. Pihlajamäki, H. Koivikko, J. Mattila, M. Mänttäri, Effect of extended exposure to alkaline cleaning chemicals on performance of polyamide (PA) nanofiltration membranes, Sep. Purif. Technol. 158 (2016) 115–123. doi:10.1016/j.seppur.2015.12.015.

[51] C.Y. Tang, Y.N. Kwon, J.O. Leckie, Effect of membrane chemistry and coating layer on physiochemical properties of thin film composite polyamide RO and NF membranes. I. FTIR and XPS characterization of polyamide and coating layer chemistry, Desalination. 242 (2009) 149–167. doi:10.1016/j.desal.2008.04.003.

[52] M. Gryta, J. Bastrzyk, D. Lech, Evaluation of fouling potential of nanofi ltration membranes based on the dynamic contact angle measurements, Polish J. Chem. Technol. 14 (2012) 97–104. doi:10.2478/v10026-012-0091-4.

[53] O. Coronell, M.I. González, B.J. Mariñas, D.G. Cahill, Ionization behavior, stoichiometry of association, and accessibility of functional groups in the active layers of reverse osmosis and nanofiltration membranes, Environ. Sci. Technol. 44 (2010) 6808–6814. doi:10.1021/es100891r.

[54] A.P. Rao, S. V. Joshi, J.J. Trivedi, C. V. Devmurari, V.J. Shah, Structure-performance correlation of polyamide thin film composite membranes: Effect of coating conditions on film formation, J. Memb. Sci. 211 (2003) 13–24. doi:10.1016/S0376-7388(02)00305-8.

[55] D. Peak, R.G. Ford, D.L. Sparks, An in Situ ATR-FTIR Investigation of Sulfate Bonding Mechanisms on Goethite, J. Colloid Interface Sci. 299 (1999) 289–299. doi:10.1006/jcis.1999.6405.

[56] P. Hintze, H. Kjaergaard, V. Vaida, J. Burkholder, Vibrational and electronic spectroscopy of sulfuric acid vapor, J. Phys. Chem. A. 107 (2003) 1112–1118. doi:10.1021/jp0263626.

[57] S.H. Kim, S.-Y. Kwak, T. Suzuki, Evidence to demonstrate the flux-enhancement mechanism in morphology-controlled thin-film-composite (TFC)membrane, Environ. Sci. Technol. 39 (2005) 1764–1770.

[58] C. Zhao, C.Y. Tang, P. Li, P. Adrian, G. Hu, Perfluorooctane sulfonate removal by nanofiltration membrane-the effect and interaction of magnesium ion / humic acid, J. Memb. Sci. 503 (2016) 31–41. doi:10.1016/j.memsci.2015.12.049.

[59] J.S. Stevens, A.C. De Luca, M. Pelendritis, G. Terenghi, S. Downes, S.L.M. Schroeder, Quantitative analysis of complex amino acids and RGD peptides by X-ray photoelectron spectroscopy (XPS), Surf. Interface Anal. 45 (2013) 1238–1246. doi:10.1002/sia.5261.

[60] I.F. Amaral, P.L. Granja, M. a Barbosa, Chemical modification of chitosan by phosphorylation: an XPS, FT-IR and SEM study., J. Biomater. Sci. Polym. Ed. 16 (2005) 1575–1593. doi:10.1163/156856205774576736.

[61] B.M. Reddy, P.M. Sreekanth, Y. Yamada, Q. Xu, T. Kobayashi, Surface characterization of sulfate, molybdate, and tungstate promoted TiO2-ZrO2 solid acid catalysts by XPS and other techniques, Appl. Catal. A Gen. 228 (2002) 269–278. doi:10.1016/S0926-860X(01)00982-6.

Supplementary information

S1. ATR-FTIR spectra for virgin and aged membrane

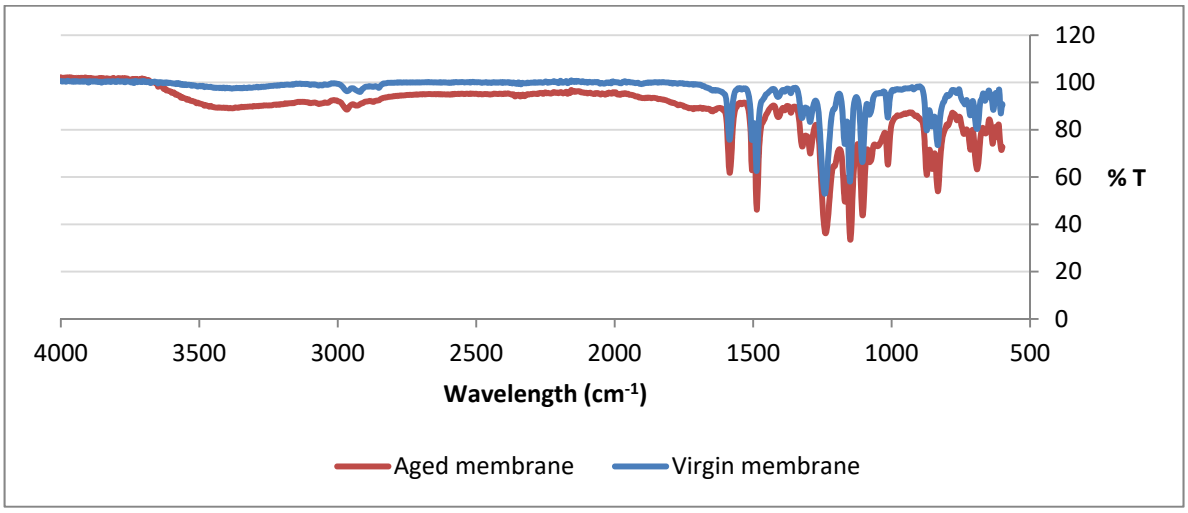

Figure S1.1. ATR-FTIR spectra for virgin and aged NF270 membranes at wave number from 4000 to 500 cm^{-1}

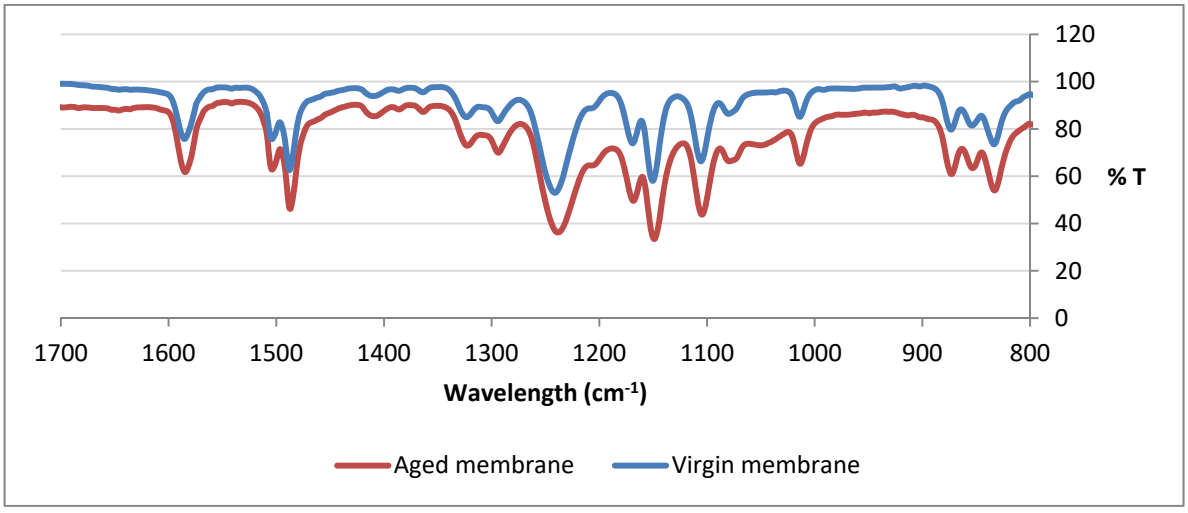

Figure S1.2. ATR-FTIR spectra for virgin and aged NF270 membranes at wave number from 1700 to 800 cm^{-1}

Table S1.1 summarizes the observed changes on polyamide layer comparing the virgin and aged membrane peak assignments.

Table S2.1. Peak assignment for NF270 membrane

Assignment	Wavenumber (cm^{-1})	Group	Vibration	Virgin NF270 (cm^{-1})	Aged NF270 (cm^{-1})
PA (piperazine polyamide)	3100	OH (carboxylic acids) NH_3^+ (amino acids)	O-H stretching N-H stretching	3099 (-1.0)	3098 -1.9
	2800	CH_3 attached to O or N	C-H stretching/bending	2800	2799

	1450	Carboxylic acid	C-O stretching O-H bending	n.d.	n.d.
	1541	Amide II	N-H bending N-C stretching	n.d.	n.d.
	1609	Aromatic amide	N-H deformation C=C ring stretching	n.d.	n.d.
	1663	Amide I band, Second amide groups	C=O stretching C-N stretching C-C-N deformation	1662,3	1661,4 (0.9)
PS (polysulphone)	1152	Sulphone	O=S=O symmetric stretching	1150.3	1149(4)(1.1)
	1244	Ethers	C-O-C stretching	1241	n.d.
	1586		C=C Phenyl group	1885.2	1584.2(1)
	1495			1494.5	(1393.5) (1)
	1106			0	1105
Foreign species (H_2SO_4, HSO_4^-, H^+)	1100	H_2SO_4	O-H stretching	n.d.	1100
	1464.7		S=O stretching	n.d.	1464.7
	894.1		S-O stretching	n.d	894.1

S2. AMD rejection data

Table S2.1. Comparison of rejection data in AMD solutions for different NF membranes

Mem. (IEP)	Feed composition (mg/L)	pH	Jv or TMP	Rejection (%)	Reference
NF270 (3)	Al^{3+}: 340, SO_4^{2-}: 4599, Zn^{2+}: 43, Ca^{2+}: 269	1.5	3.2–46 µm/s	Al^{3+}: 64 – 89, SO_4^{2-}: 35 – 59, Zn^{2+}: 63 – 90, Ca^{2+}: 63 – 90, H^+: -6.4 – 9.21	This work
	Al^{3+}: 343, SO_4^{2-}: 3216, Zn^{2+}: 43, Ca^{2+}: 240	1.9	1.4 – 45 µm/s	Al^{3+}: 78 – 97, SO_4^{2-}: 57 – 77, Zn^{2+}: 77 – 96, Ca^{2+}: 76 – 97, H^+: -19 / -4	This work
	Al^{3+}: 335, SO_4^{2-}: 2563, Zn^{2+}: 43, Ca^{2+}:240	2.5	3.4 – 49 µm/s	Al^{3+}: 69 – 88, SO_4^{2-}: 62 – 83, Zn^{2+}: 68 – 89, Ca^{2+}: 68 – 87, H^+: -38 / -2.5	This work
	Al^{3+}: 559, SO_4^{2-}: 9389, Zn^{2+}: 46, Ca^{2+}: 24, Cu^{2+}: 38, La^{3+}: 10, Pr^{3+}: 10, Nd^{3+}: 10, Sm^{3+}: 10, Dy^{3+}: 10, Yb^{3+}: 10	1	5.8 – 24.8 µm/s	Al^{3+}: 99, SO_4^{2-}: 39 – 48, Zn^{2+}: 99.6, Ca^{2+}: 98.9 – 99.8, Cu^{2+}: 99.5, La^{3+}: >99.8, Pr^{3+}: >99.8, Nd^{3+}: >99.8, Sm^{3+}: >99.8, Dy^{3+}: >99.8, Yb^{3+}: >99.8, H^+: -6.4 – 5.8	This work
	Ca^{2+}: 480, Cu^{2+}: 410, Mg^{2+}: 770, Mn^{3+}: 440, Na^+: 2000, SO_4^{2-}: 6900	1.5 - 4.6	32 L/m^{2}h 22 bar	Ca^{2+}: 96 – 91, Cu^{2+}: 96 – 89, Mg^{2+}: 97 – 94, Mn^{3+}: 97 – 94, Na^+: 38 – 45, S^{2-}: 89 – 96	[18]
TS80 (3)		1.5 – 5.5	35 L/m^{2}h 19 bar	Ca^{2+}: 98, Cu^{2+} 97, Mg^{2+}: 98 Mn^{2+}: 98, S^{2-}: 98, Na^+: 97	[18]
Envig D11	SO_4^{2-}: 1430, Cl^-: 418, Na^+: 344 Ca^{2+}: 354	2	3 – 20 bar	SO_4^{2-}: -13, Cl^-: 8, Na^+: 8, Ca^{2+}: 75	[20]
Envig				SO_4^{2-}: -65, Cl^-: 12, Na^+: 0, Ca^{2+}: 74	[20]

D12					
NF90 (4.3)				SO_4^{2-}: 9, Cl^-: 88, Na^+: 92, Ca^{2+}: 96	[20]
NF70 (3-3.5)				SO_4^{2-}: 99, Cl^-: 90, Na^+: 95, Ca^{2+}: 97	[20]
Nitto Denko CTC1				SO_4^{2-}: 47, Cl^-: 24, Na^+: 31, Ca^{2+}: 81	[20]
DK-4040F	Ni^{2+}: 17, Cu^{2+}: 79, Zn^{2+}: 18, Pb^{2+}: 10, SO_4^{2-}: 36, NO_3^-: 107 Cl^-: 530, Na^+: 653	3	0.2 – 1.1 MPa	Ni^{2+}: 93, Cu^{2+}: 93, Zn^{2+}: 94, Pb^{2+}: 95,	[15]
NF99	Cu: 2298, Fe: 628, Mn: 225, Ca: 326, Mg: 630, Na:7, Al: 1139, SO_4: 14337	2.7 – 2.5	20 – 30 bar	Cu: 99.9, Fe: 99.9 , Mn: 99.9, Ca: 99.9, Mg: 99.6, Na: 87.7 , Al: 99.9, SO_4: 98.6, pH: 2.6	[16]
GE				Cu: 99.3, Fe: 99.5, Mn: 99.4, Ca: 99.3, Mg: 99.4, Na: 82,5, Al: 99.5, SO_4: 98.6, pH 2.6	[16]
DK				Cu: 50– 82, Fe: 84 – 92 Mn: 61 – 82, Ca: 60– 82, Mg: 61 – 92, Na: 34– 56, Al: 80 – 90, SO_4: 73 – 87, pH: 2.8 - 2.3	[16]

S3. Contact angle

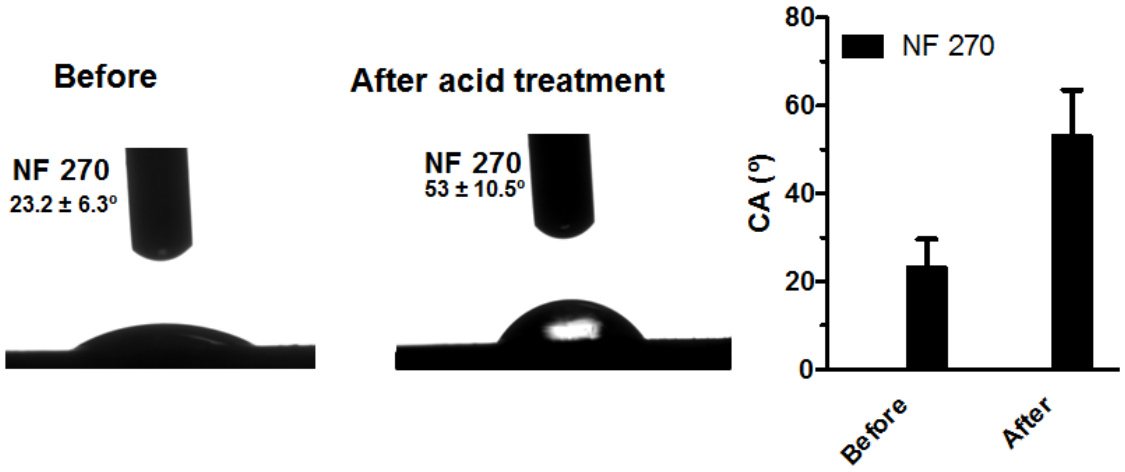

Figure S3.1. Contact angle data for NF270 before and after acid treatment, with corresponding water droplet images.

S4. High resolution XPS spectra for virgin and aged NF270

Table S4.1. XPS spectra for C 1s, O 1s and N 1s for (a) virgin membrane and (b) for the aged membrane

	Virgin membrane	Aged membrane

C (1s)	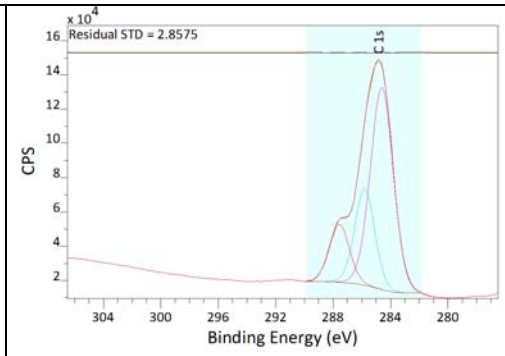	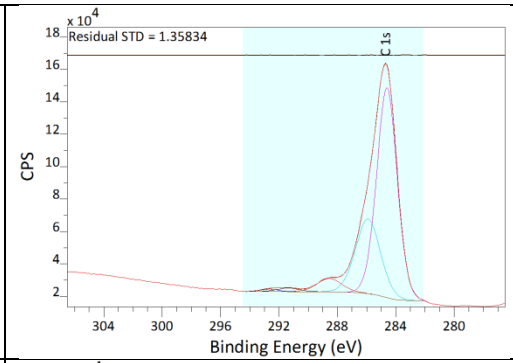
O (1s)	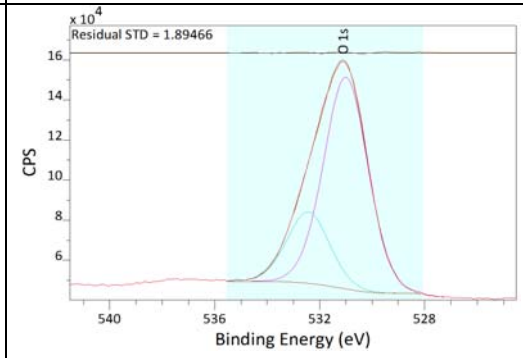	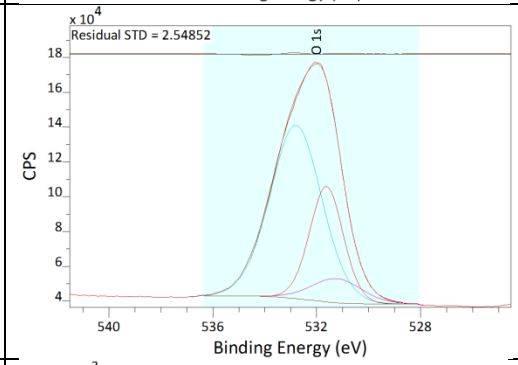
N (1s)	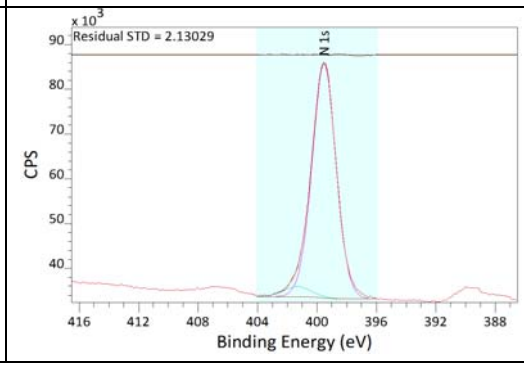	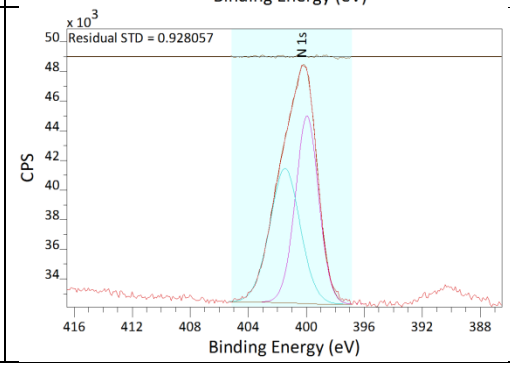

Table S4.2. Binding energies and relatively amount of functional groups for virgin and aged membrane

	Virgin membrane		Aged membrane	
	E_B (eV)	%	E_B (eV)	%
C (1s)	72.5 %		66.0 %	
C-C,C-H, C=C	284.6	60.1	284.6	65.0
C-O, C-N	285.8	24.9	285.9	28.2
C=O-N, N=C, C=O	287.6	15	288.6	5.0
Saturated, π bond			292.7	0.7
Saturated, π bond			291.4	1.2
N (1s)	16.8 %		23.0 %	
C-N, C=N, O=C-N	399.5	95.3	399.9	51.6
$-NH_3^+$, $-NH_2R^+$	401.3	4.7	401.5	48.4
O (1s)	10.7 %		4.9 %	
O=C-N, C=O, C-O	531	75.6	531.2	8.7
H···O=C-N, O=C-O	532.4	24.4	532.8	63.7
SO_4^{2-}			531.6	27.6